Reconstruction of a Tornado Disaster Employing Remote Sensing Techniques: A Case Study of the 1999 Moore, Oklahoma Tornado

by

Melissa A. Wagner

A Thesis Presented in Partial Fulfillment
of the Requirements for the Degree
Masters of Arts

Approved April 2011 by the
Graduate Supervisory Committee:

Randall S. Cerveny, Co-Chair
Soe W. Myint, Co-Chair
Elizabeth A. Wentz
Anthony J. Brazel

ARIZONA STATE UNIVERSITY

May 2011

ABSTRACT

Remote sensing has demonstrated to be an instrumental tool in monitoring land changes as a result of anthropogenic change or natural disasters. Most disaster studies have focused on large-scale events with few analyzing small-scale disasters such as tornadoes. These studies have only provided a damage assessment perspective with the continued need to assess reconstruction. This study attempts to fill that void by examining recovery from the 1999 Moore, Oklahoma Tornado utilizing Landsat TM and ETM+ imagery. Recovery was assessed for 2000, 2001 and 2002 using spectral enhancements (vegetative and urban indices and a combination of the two), a recovery index and different statistical thresholds. Classification accuracy assessments were performed to determine the precision of recovery and select the best results. This analysis proved that medium resolution imagery could be used in conjunction with geospatial techniques to capture recovery. The new indices, Shortwave Infrared Index (SWIRI) and Coupled Vegetation and Urban Index (CVUI), developed for disaster management, were the most effective at discerning reconstruction using the 1.5 standard deviation threshold. Recovery rates for F-scale damages revealed that the most incredibly damaged areas associated with an F5 rating were the slowest to recover, while the lesser damaged areas associated with F1-F3 ratings were the quickest to rebuild. These findings were consistent for 2000, 2001 and 2002 also exposing that complete recovery was never attained in any of the F-scale damage zones by 2002. This study illustrates the significance the biophysical impact has on recovery as well as the effectiveness of using medium resolution imagery such as Landsat in future research.

ACKNOWLEDGEMENTS

I would like to thank the following people: Kimme DeBiasse for formatting help, Barbara Trapido-Lurie for helping me beautify my maps and tailor the information to my audience, Shai Kaplan for bouncing remote sensing ideas off of, and Chris Galetti for atmospheric correction and the use of his labtop; only crisp and beautiful images from now on. I am extremely fortunate to Dr. Brazel who took an interest in my application and offered sage advice. Thank you Dr. Elizabeth Wentz, for letting me camp out during your class to work on my research, your poignant insights and support, and believing in me. While I know I tried the patience of Dr. Soe Myint, I am forever indebted to you for my remote sensing education, introduction to tornado damage assessment and brilliant guidance in my research. To Dr. Randall Cerveny, may I never hear the phrase "If it was easy, everybody would do it." Thank you for letting me be the headstrong, obstinate student I am, but most importantly for never giving up on me and coaxing me along the way when I seriously doubted my abilities. My best friends, Kym Suthers, Heidi Berardi and Tracy Schirmang for their support, editing capabilities including untangling the words in my head and encouragement to pursue my passion regardless of the difficulty. To my children, Paix, Cierra, Hugo and Helen, follow your dreams, live passionately and never set limits. Education will take you wherever you envision yourselves. Lastly, but most importantly, my husband, Joe Wagner, without your support none of this would be possible and understanding this is only the beginning.

TABLE OF CONTENTS

Page

LIST OF TABLES vi

LIST OF FIGURES vii

1. INTRODUCTION 1

1.1 Introduction 1

1.2 Research Question 2

1.3 Background 5

1.4 Framework 6

2. LITERATURE REVIEW 8

2.1 Theory of Hazards 8

2.2 Damage Assessment 17

2.3 Aerial photography 21

2.4 Remote Sensing 22

2.5 Conclusion 30

3. STUDY, DATA AND METHODS 32

3.1 Introduction 32

3.2 Study Area 32

3.3. Data and Data Preparation 35

3.4. Digital Analysis 39

3.5 Change Vector Analysis 46

3.6 Conclusion 47

4. RESULTS 49

4.1 Introduction 49

4.2 Assessment of New Indices and Initial Impact of Tornado 49

4.3 Performance of the Recovery Index 55

4.4 Annual Reconstruction and Recovery Rates 69

4.5 Recovery Rates as a Function of the Fujita Scale 76

4.6 Change Vector Analysis 84

4.7 Conclusion 84

5. DISCUSSION 86

5.1 Introduction 86

5.2 Remotely Sensed Data and Recovery Index 87

5.3 Recovery Rates as a Function of F-scale 92

5.4 Conclusion 97

6. SUMMARY AND CONCLUSION 99

6.1 Summary 99

6.2 Suggestions for Future Research 100

6.3 Significance 101

REFERENCES 103

LIST OF TABLES

Table Page

1. Specific satellite imagery utilized in the study 36

2. List of Threshold Values of 0.5, 1.0, 1.5 standard deviations to define recovery for each index and year. 45

3. Sampled Means of Different Land Cover Classes. 50

4. Accuracy Assessments listed by Index, Standard Deviation Threshold and Year. 66

5. Averaged Accuracy Assessments listed by Index and Standard Deviation Threshold. (Overall = Overall accuracy, Prod. = Producer's accuracy, User's = User's Accuracy) 67

6. Annual Recovery Rates listed by Index, Threshold (Thres.) and Year. 71

7. Recovery Rates for F-scale zones listed by Index, Threshold (Thres.) and Year. 78

8.Recovery Rates for F-scale zones listed by Index, Threshold and Year 79

9. List of Land Class Types and Associated Land Use Changes..... 82

LIST OF FIGURES

Figure Page

Fig. 1. Map of recorded tornado locations during the May 3, 1999 Tornado Outbreak in Central Oklahoma..... 35

Fig. 2. Map displaying county boundaries in the state of Oklahoma and the study area outlined in red. 38

Fig. 3. False Color Composite of the Study Area displaying Band 4 in red, Band 3 in green and Band 2 in blue. 38

Fig. 4. 1998 Urban Index showing the transect of different land covers of the 1999 Moore, Oklahoma Tornado-impacted region a year before the tornado disaster. 50

Fig. 5. Reflectance Curves for Coupled Vegetation and Urban Index, Normalized Difference Vegetative Index, Soil Adjusted Vegetative Index, Shortwave Infrared Index, Urban Index.. 51

Fig. 6. 1999 Coupled Vegetation and Urban Image (CVUI) of the Moore, Oklahoma Tornado-impacted region. 52

Fig. 7. 1999 Urban Index (UI) of the Moore, Oklahoma Tornado-impacted region. 53

Fig. 8. 1999 Normalized Difference Vegetative Index (NDVI) of the Moore, Oklahoma Tornado-impacted region. 53

Fig. 9. 1999 Soil Adjusted Vegetative Index (SAVI) for the Moore, Oklahoma Tornado-impacted region. 54

Figure Page

Fig. 10. 1999 Shortwave Infrared Vegetative Index (SWIRI) for the Moore, Oklahoma Tornado-impacted region. 54

Fig. 11. 1999 Urban Index showing the transect for 1999 Moore, Oklahoma Tornado-impacted region right after the tornado disaster. 55

Fig. 12. Transect of Damaged Area affected by the 1999 Moore, Oklahoma 4.3..... 55

Fig. 13. 2000 Recovery Image of Coupled Vegetation and Urban Image CVUI of the 1999 Moore, Oklahoma Tornado-impacted region. 57

Fig. 14. 2001 Recovery Image of Coupled Vegetation and Urban Image CVUI of the 1999 Moore, Oklahoma Tornado-impacted region. 58

Fig. 15. 2002 Recovery Image of Coupled Vegetation and Urban Image CVUI of the 1999 Moore, Oklahoma Tornado-impacted region. 58

Fig.16. 2000 Recovery Image of the Urban Index (UI) of the 1999 Moore, Oklahoma Tornado-impacted region. 59

Fig. 17. 2001 Recovery Image of the Urban Index (UI) of the 1999 Moore, Oklahoma Tornado-impacted region. 59

Fig.18. 2002 Recovery Image of the Urban Index (UI) of the 1999 Moore, Oklahoma Tornado-impacted region. 60

Fig. 19. 2000 Recovery Image of Normalized Difference Vegetative Index (NDVI) of the 1999 Moore, Oklahoma Tornado-region. 60

Figure Page

Fig. 20. 2001 Recovery Image of Normalized Difference Vegetative Index (NDVI) of the 1999 Moore, Oklahoma Tornado-impacted region. 61

Fig. 21. 2002 Recovery Image of Normalized Difference Vegetative Index (NDVI) of the 1999 Moore, Oklahoma Tornado-impacted region. 61

Fig. 22. 2000 Recovery image of Soil Adjusted Vegetative Index (SAVI) of the 1999 Moore, Oklahoma Tornado-impacted region. 62

Fig . 23. 2001 Recovery image of Soil Adjusted Vegetative Index (SAVI) of the 1999 Moore, Oklahoma Tornado-impacted region. 62

Fig. 24. 2002 Recovery image of Soil Adjusted Vegetative Index (SAVI) of the 1999 Moore, Oklahoma Tornado-impacted region. 63

Fig. 25. 2000 Recovery image of the Shortwave Infrared Index (SWIRI) of the 1999 Moore, Oklahoma tornado-impacted region..... 63

Fig. 26. 2001 Recovery image of the Shortwave Infrared Index (SWIRI) of the 1999 Moore, Oklahoma tornado-impacted region..... 64

Fig.27. 2002 Recovery image of the Shortwave Infrared Index (SWIRI) of the 1999 Moore, Oklahoma tornado-impacted region. 64

Fig. 28. Map of the 1999 impacted region showing recovered and damaged regions for 2000, 2001 and 2002 using the Coupled vegetative and urban index and 1.0 standard deviation threshold. 72

Figure Page

Fig. 29. Map of the 1999 impacted region showing recovered and damaged regions for 2000, 2001 and 2002 using the coupled vegetative and urban index and 1.5 standard deviation threshold. 73

Fig. 30. Map of the 1999 impacted region showing recovered and damaged regions for 2000, 2001 and 2002 using the Shortwave Infrared Index (SWIRI) and 1.0 standard deviation threshold. 73

Fig. 31. Map of the 1999 impacted region showing recovered and damaged regions for 2000, 2001 and 2002 using the Shortwave Infrared Index (SWIRI) and 1.5 standard deviation threshold. 74

Fig. 32. Map of the 1999 Moore Oklahoma Tornado-impacted region showing recovered and damaged regions for 2000, 2001 and 2002 using the Urban Index (UI) and 1.0 standard deviation threshold. 75

Fig. 33. Map of the 1999 Moore Oklahoma Tornado-impacted region showing recovered and damaged regions for 2000, 2001 and 2002 using the Urban Index (UI) and 1.5 standard deviation threshold. 75

Fig. 34. Graph for the 1999 Moore Oklahoma Tornado-impacted region displaying annual recovery rates for 2000, 2001 and 2002 in percent by F-scale intensity as established by the recovery index. 80

Fig. 35. Graph for the 1999 Moore Oklahoma Tornado-impacted region displaying F-scale recovery rates in percent for 2000, 2001 and 2002 as established by the recovery index..... 81

Figure Page

Fig. 36. Change Vector Analysis Map of the 1999 Moore Oklahoma Tornado-impacted region for 2000 showing different land class changes..... 82

Fig. 37. Map of the 1999 Moore Oklahoma Tornado-impacted region showing the magnitude of changes for 2000 using change vector analysis..... 83

Fig. 38. Map of the 1999 Moore Oklahoma Tornado-impacted region showing the magnitude of changes for 2001 using change vector analysis..... 84

Fig. 39. Map of the 1999 Moore Oklahoma Tornado-impacted region showing the magnitude of changes for 2002 using change vector analysis..... 84

1. Introduction

1.1 Introduction

Hazard studies have recognized remote sensing technology as a powerful tool in damage assessment and recovery analysis. These methods have been extensively used in monitoring land cover changes resulting from natural and anthropogenic processes as a result of its ubiquitous coverage, regular data collection and repeatable independent analyses (Magsig et al. 2000, Yuan et al. 2002, Myint et al. 2008, Myint et al. 2008b, Mura et al. 2008). Through the manipulation of multispectral data, damaged areas can be detected by the alterations of spectral signatures in land cover features caused by a natural disaster (Bentley et al. 2002, Yuan et al. 2002, Jedlovec et al. 2006). Depending on the technology selection and resolution employed, different damage levels can be discerned, thus serving as a low cost alternative to aerial photography or intensive ground surveys (Yuan et al. 2002, Jedlovec et al. 2006, Myint et al. 2008, Myint et al. 2008b).

Improvements in resolution and image processing techniques have recently made remote sensing an increasingly popular method for studying disaster impacts (Yuan et al. 2002). Finer resolutions have improved the discernment of small-scale features; yet, drawbacks exist as the result of more intensive algorithms and increasing processing times for imagery analysis. While detailed damage information can be obtained on individual objects with finer resolution, this imagery may fail to capture the extent of the impacted areas due to much smaller scenes. Medium resolution imagery such as Landsat TM and

Landsat ETM+ considers ground features together with the bigger pixel size, thereby providing a top-view assessment. With the development of an effective series of image processing algorithms, this imagery could better capture the chaotic nature of damaged areas than fine resolution imagery.

Most disaster studies have focused on issues of vulnerability and recovery with large-scale events such as floods, earthquakes, tsunamis and hurricanes. While tornado damage may be viewed as only affecting a small concentrated area, there is still a need to examine the impacts tornadoes have on society. Depending on the intensity of the tornado and the infrastructure within its path, the magnitude of damage can actually be greater than large-scale events.

Understanding all aspects of a disaster from its impact to recovery is crucial in implementing effective mitigation strategies for future events (Uitto 1998, Cutter 2003). More recently, issues of social vulnerabilities and recovery have been brought to the forefront with such notable disasters as the December 2004 Tsunami, Hurricane Katrina and Haitian Earthquake. While these factors affect society's ability to recover, the scope and magnitude of the disaster still plays a critical role in societal recovery and resiliency (Cutter 1996, Cutter et al. 2003). Examining disparities in reconstruction due to the biophysical impact can provide valuable information in the degree of restoration and recovery. This knowledge would lead to better decision-making policies that could reduce disparities in the reconstruction process within the most severely damaged areas.

1.2 Research Question

Hazard studies have shown that the effects of a natural disaster to a society are not uniform. The scope and magnitude of the disaster can have a lasting impact based on the amount of damage sustained, thus affecting the ability to fully recover (Dacy and Kunreuther 1969, Haas et al. 1977, Uitto 1998, Yasui 2007, Fitch et al. 2010, Aldridge 2011). Most disaster studies have assessed the initial damages and reconstruction of large-scale events like hurricanes, earthquakes and tsunamis, but very few hazard studies have examined the lasting impacts of small-scale events like tornadoes.

Remote sensing techniques have more recently been employed in the few tornado disaster studies. Their research (Magsig et al. 2000, Yuan et al. 2002, Jedlovec et al. 2006, Myint et al. 2008, Wilkinson and Crosby 2010) only examined the initial impact with regards to the extent and severity of damages. Another study by Myint et al 2008b expanded on previous damage studies by categorizing the different F-scale ratings through geospatial techniques. However, no known study has employed geospatial methods as a means to objectively capture the reconstruction of a tornado disaster.

This study attempts to answer the following research questions:

- How effective are geospatial techniques in assessing recovery and reconstruction using medium resolution imagery (e.g. Landsat TM or Landsat ETM+)?
- Are recovery rates uniform with regard to damage level (e.g., Fujita scale)?

These questions can be addressed through a study involving remote sensing and GIS technologies. My hypothesis is that recovery rates are directly dependent on the level of the damage sustained, as measured by the Fujita Scale. Consequently, employing an analysis involving geospatial techniques will assess the initial tornado damage and reconstruction using Landsat-TM and Landsat ETM+ imagery before and several years after the disaster.

This analysis focuses on the 1999 Moore, Oklahoma tornado event of May 3, 1999. The tornado first touched down in the central portion of Grady County and traveled 38 miles before dissipating on the eastern side of Oklahoma City in Oklahoma County. Within the path, the cities of Moore and Bridge Creek sustained the most damage based on its dense infrastructure and inferred intensity rating of F5 on the Fujita Scale. The impact of the 1999 Moore, Oklahoma tornado was 36 people lost their lives and damages exceeded 1.6 billion US dollars making it one of the costliest tornadoes in US history (Brooks and Doswell 2002, NCDC 2010).

For the Moore, Oklahoma tornado, image-processing techniques were performed on Landsat TM imagery of 1998, 1999, 2000, 2001, and 2002. These images were normalized the data to reduce spatial and temporal variations not associated with the tornado (Singh 1989, Myint et al. 2008). Spectral enhancements and temporal differencing were also employed to discern changes attributed to the tornado. Both damaged and recovered areas were classified using a recovery index and spatially analyzed in conjunction with F-scale zones

determined by National Weather Service ground surveys. Recovery rates were then computed for each F-scale zone.

By examining the recovery rate of the Moore, Oklahoma tornado, the hypothesis is that the response to such a disaster is not uniform, but rather a function of the biophysical impact. By revealing these issues of disparity, future studies can use this knowledge to implement better planning methods and mitigation strategies in the most impacted regions that can be expected to reduce the recovery period for those groups most impacted by the storm.

1.3 Background

After a tornado event, damage surveys are conducted to assess the extent of the damaged area and classify the intensity of the tornado on the Fujita Scale. Since no direct measurements can be made, the intensity of the tornado must be inferred by correlating the level of damage and estimated wind speeds (Marshall 2002, McDonald 2002, Doswell et al. 2009). Ratings on this scale range from F0 to F5 where an F5 rating corresponds to the most incredible degree of damage (Fujita 1971, 1981, 1993, Grazulis 1991). Recently, this scale was modified to reduce the subjectivity of the scale and renamed to the Enhanced Fujita Scale with EF ratings (McDonald 2002). However, this change was made several years after the tornado, therefore, I used the classified tornado ratings in the context of the original Fujita Scale.

To research recovery, remote sensing methods of spectral enhancements, temporal differencing and series of image processing algorithms were used. Spectral enhancements can discern damages not readily visible to the human eye

either by either reducing data redundancy (e.g. principle components analysis (PCA)) or algebraically manipulating bands (e.g. band ratioing) on a single image. Temporal differencing differs from spectral enhancements in a new image is produced based on the subtraction two images of the same area to highlight changed areas (Singh 1989, Myint et al. 2008). With these images, a series of image processing techniques were employed to classify damaged and recovered regions using a recovery index and different thresholds. The top-performing results were spatially analyzed in conjunction with F-scale damage zones to derive F-scale recovery rates for the specific recovery years of 2000, 2001, and 2002.

1.4 Framework

To accomplish this geospatial assessment of the reconstruction of the 1999 Moore, Oklahoma Tornado, my thesis is organized as follows:

Chapter 2 provides a detailed literature review on issues pertaining to both hazards and remote sensing components. This section is divided into discussions of biophysical and social vulnerability factors concerning the initial impacts and the recovery process. This chapter also examines previous remote sensing studies for both large-scale events and small-scale events with regards to damage assessments and recovery analysis. By reviewing both hazard perspectives and geospatial techniques, this section aims to produce a comprehensive view of the recovery process after a natural disaster.

Chapter 3 discusses the study area, data selected for the analysis, and methods involved in assessing reconstruction. Limitations inherent in the data

and quality control methods necessary for successful change detection are addressed. Geospatial techniques for analyzing the reconstruction process are discussed as well as how recovery rates were calculated.

In Chapter 4, the results produced from the methods are presented. Detected changes in terms of damaged and recovered regions are discussed. Both recovery rates and spatial disparities are analyzed and presented.

In Chapter 5, the results from Chapter 4 are interpreted with the key findings discussed. Critical findings regarding geospatial assessments of the reconstruction of a tornado and spatial disparities are explained.

In Chapter 6, the key findings are summarized and fundamental conclusions of this thesis are offered. Suggestions for future work are highlighted with the significance of this work closing this research.

2. Literature Review

2.1 Theory of Hazards

When a natural process or phenomenon negatively impacts society, that event concentrated in time and space is labeled a natural disaster (Turner 1976, Alexander 1991). Unlike a disaster, a natural hazard is the perceived threat or likelihood of loss from a future occurrence of suffering an adverse effect where human vulnerability intersects with the biophysical processes (Fussel 2007). At this intersection, the impacts of a disaster can either be attenuated or amplified depending on the type of implemented mitigation strategies and underlining social characteristics (Alexander 1991, Cutter 2003, Turner et al. 2003, Cutter 2008). Understanding how the biophysical process integrates with the socio-environment is crucial in not only measuring the sensitivity of the impact, but also in determining the recovery and resiliency of the region (Cutter 1996).

The emergence of hazard studies in geography began with Barrows (1923) by taking an ecological approach to human adaptation and the environment (Alexander 1991). He analyzed spatial and temporal aspects of risk and susceptibility, but only focused on high magnitude events. Brookfield (1964) pointed out contradictions with perceptions and responses to hazards calling to expand the scope of how it relates to the socio-environment system (Grossman 1977, Alexander 1991). Following Brookfield, Hewitt and Burton (1971) recognized human elements in disasters in addition to geophysical components (Cutter et al. 2003). Further research by Burton et al. 1978 stressed viewing hazards as ongoing phenomena within socio-environment systems, thus

advancing hazards research beyond causal agents. Building on this ecological perspective, Timmerman (1981) argued that disasters were largely functions of societal vulnerabilities in terms of sensitivity and resiliency of a system (Cutter 1996, Adger 2006, Fussel 2007).

Hazard research can be broken down into aspects of vulnerability and resiliency (Klein et al 2003, Adger 2006, Zhou et al. 2010). Vulnerability broadly defined is the potential for loss (Cutter 1996, Cutter et al 2003, Etkin et al. 2004, Berkes et al. 2005) and can be further subdivided into physical and social components. Physical vulnerability, or risk, is the likelihood of experiencing some adverse effect based on the geophysical characteristics of the environment, whereas, social vulnerability is concerned with whom or what is susceptible to the loss (Turner 1976, Turner et al. 2003, Cutter et al 2003; 2008). Resiliency, unlike risk and social vulnerability, is concerned with post-event impacts and measures how an individual or group responds and recovers once the disaster has occurred (Cutter 1996, Turner et al. 2003, Cutter et al. 2008).

In hazard studies, risk loosely defined is the likelihood of the phenomena occurring with an undesirable outcome (Brooks et al. 2003). From the beginning of hazard research, risk has been viewed as the distribution from some hazard condition (Burton et al. 1978, Alexander 1991, Cutter 1996). Here, inhabiting in hazard zones and the degree of loss is associated with a regionalized event based on known past occurrences (Cutter 1996, Brooks et al. 2003). Within these zones, risk can either be attenuated or amplified depending on the magnitude, duration,

impact and onset of the event as well as any mitigation strategies already in place (Cutter 1996, Mileti 1999, Mitchell 1999, Uitto 1999, Cutter et al. 2008).

Social vulnerability like risk is also concerned with the antecedent conditions of the event except the focus shifts from the physical characteristics of the hazard to social concerns in terms of whom or what is exposed to the loss (Turner 1976, Turner et al. 2003, Cutter et al. 2003; 2008). This concept views the hazard draped over society as a given and investigates who or what would be most adversely affected based on social conditions (Cutter et al. 2003; 2008). Here, disadvantaged groups are more vulnerable to certain hazards based on lower socioeconomic means, lack of resources and poor housing quality regardless of the distance to the damaging source (Burton et al. 1993, Cutter 2000). The disparaging impacts of a disaster can be attributed to social inequalities based on factors of age, race, ethnicity, socioeconomic status, political institutions and other social variables (Liverman 1990, Burton et al. 1993, Blaikie et al 1994, Cutter 1996; 2000, Cutter et al. 2003). Recent examples of these inequalities have been noted with the impact and recovery of Hurricane Katrina and the 2004 Tsunami (Finch et al. 2010)

In addition to the aforementioned factors, social vulnerability takes into account how the built environment is constructed from a generalized paradigm. This aspect of social vulnerability has essentially evolved from engineering mitigation strategies that have recognized shortcomings in dwelling types, certain types of infrastructure, and urban versus rural settings. Certain dwelling types and infrastructure have proven to be a key factor in disaster impacts based on

material composition and number of housing units within a dwelling as shown by Uitto 1998, Mitchell 1999 and Mileti 1999. In particular, mobile homes and manufacturing houses are far more susceptible to damage than the typical framed house even when anchored to a foundation (Marshal 2002, Pan 2002). While these dwellings only make up about 8% of the housing market, approximately 40% of the tornado fatalities occur in these structures (Simmons 2007). These marginalized residents comprised of elderly and low-income families are 10 to 15 times more likely to die in a tornado disaster than the occupants of a single family framed home (Brooks and Doswell 2002, Simmons 2007).

Urban settings can also compound the effects of a disaster due to higher density and societal trends. Higher densities in the urban environment increase the conditional risk for fatalities by generating more debris and consequently projectiles (Brooks and Doswell 2002, Marshall 2002, Pan 2002, DeSilva et al. 2008). This produces a domino effect in damage patterns and can often lead to structural failure of surrounding structures in wind driven disasters and flooding events (Brooks and Doswell 2002, Marshall 2002, Pan 2002, Brooks et al. 2003, DeSilva et al. 2008). In the case of tornado disasters, both structural failures and wind-driven projectiles are responsible for the leading cause of death (Brooks and Doswell 2000, Boruff et al. 2003).

Societal trends in urban settings also pose a higher risk based on growing populations. With an increased demand for housing and service buildings, rushed decision making in planning and construction could affect the integrity of the structure and consequently increase the building's vulnerability (Uitto 1998,

Marshall 2002, Brooks et al. 2003, Cutter 2003, Doswell 2005, Cutter et. al 2008, Wentz et al. 2009). The presence of such vulnerable structures within this environment could compromise the integrity of nearby buildings, thereby producing a larger damage field (Uitto 1998, Marshall 2002, Brooks et al. 2003, Cutter 2003, Doswell 2005, Cutter et. al 2008, DeSilva et al. 2008, Wentz et al. 2009). However, rural settings could just as vulnerable as the urban environment due to the lack of building code enforcement necessary to ensure their structural integrity despite their sparse spacing (Cross 2001, Cutter 2003).

Another social vulnerability factor that should be considered is hazard perception. (Preston et al. 1983, Alexander 1991, Donner 2007). Due to variations within society, perception differences arise based on levels of interest and the ability to implement protective measures (Donner 2007). How this threat is perceived affects their anticipated responses and consequently the magnitude of the impact (Preston et al. 1983, Alexander 1991, Cutter 1996, Donner 2007). Additionally, perception in terms of public apathy contributes to be a major factor in how prepared a society is due to long intervals between high magnitude events or frequent exposure to low impact events that become integrated within the culture (Preston et al 1983, Alexander 1991, Cutter 1996, Brooks and Doswell 1998; 2002, Doswell 2005). Perceived psychological distances and imagined boundaries drawn around the threat can also foster a false sense of security, thereby affecting the level of preparedness and consequently the degree of impact (Davis 2003).

Another aspect that has been evolving over recent years is place-based vulnerabilities. This dimension of vulnerability fuses the biophysical and social factors together to examine the most vulnerable subgroups within a geographic region (Liverman 1990, Cutter 1996). Certain places or sites can exhibit higher degrees of vulnerability based on the spatial clustering of social and biophysical characteristics (Cutter et al. 2000). This paradigm seeks not only to understand the local manifestation of vulnerability, but also the influence of larger factors operating on bigger scales (Cutter 1996, Cutter et al. 2000, Turner et al. 2003, Cutter et al. 2008). As a result, this view has moved hazard studies away from the fragmented or specialized approach common in the local or regional level to a more integrative approach (Blaikie and Brookfield 1987, Wilhite and Easterling 1987, Mitchell et al. 1989, Lewis 1987; 1990, Liverman 1990, Degg 1993, Longhurst 1995, Cutter 1996).

In addition to vulnerability, another core aspect studied in hazard research is resiliency. This concept measures how well a system can handle stress by focusing on the post-disaster responses and coping capacities of individuals or groups (Cutter 1996, Turner et. al 2003, Cutter et. al 2008, Zhou et al. 2010). As noted by Cutter et al. 2008, "Resiliency incorporates the capacity to reduce or avoid losses, contain the effects of disasters, and recover with minimal social disruptions" (Buckle et al. 2000, Manyena 2006, Tierney and Bruneau 2007, Cutter et al. 2008, p 600). This concept considers both pre-disaster mitigation and post-disaster strategies with the notion that a well-designed and resourceful system can handle the external stresses of an event and still maintain its integrity

(Adger 1997, Klein et al. 2003, Bruneau et al. 2003, Berkes et al. 2005, Tierney and Bruneau 2007, Cutter et al. 2008).

The relationship between resiliency and vulnerability has been argued within the discipline based on how resiliency is conceptualized. Traditionally, hazard studies have nested resiliency within vulnerability based on defining resiliency as an outcome or coping mechanism to the disaster (Cutter 1996). Other researchers, more in lined with socio-ecologists, treat vulnerability and resiliency as separate and opposite concepts (Turner et al. 2003). With this paradigm, resiliency is treated as a process by which a system modifies and copes with the aftermath based on adaptive capacities and knowledge gained (Cutter et al. 2008, Zhou et al. 2010). The last paradigm does not discriminate between resiliency as a process or outcome, but instead links these two concepts through a dynamical feedback with the ideology that a more resilient society will be less vulnerable and vice versa (Cutter 1996). While this conceptualization has been growing in popularity, problems exist in both measuring and delineating between these core aspects (Cutter et al. 2008).

Issues in assessing vulnerability and resiliency also exist when dealing with spatial and temporal components. In terms of scale, attributes selected to measure a particular variable may not always transcend across other scales without losing some detailed information (Turner et al. 2003). In regards to temporal aspects, the true onset of an event may be difficult to define depending on measurement unit and scale (Turner et al. 2003, Cutter et al. 2008). In addition to identifying the impact, the declaration of recovery can be somewhat ambiguous

as other factors or outside scale influences can affect the reconstruction process (Cutter et al. 2008).

After the disaster has occurred, there are two generalized phases within the disaster management cycle. The first phase deals with the initial consequences of the disaster in terms of emergency responses including rescues, evacuations, temporary shelters and damage assessments (Alexander 2000, Carter 1991, Quarantelli 1998, Dunford and Li 2011). The second phase, recovery, incorporates both short-term reconstruction and long-term planning. The short-term reconstruction consists of repairing and rebuilding damaged housing and infrastructure that could last up to three years, while long-term recovery pertains to economic development and long-term mitigation plans (Alexander 2000, Carter 1991, Quarantelli 1998, Dunford and Li 2011). Ideally, these two recovery concepts should overlap in the rebuilding phase to improve the resiliency of the impacted society from future events (Burby 2001).

Focusing on short-term recovery, reconstruction rates depend on the magnitude of the biophysical impact as well as social vulnerability factors. Dacy and Kunreuther (1969) initially noted that the rate of recovery was mainly attributed to the magnitude of damage sustained in the recovery assessment of the 1964 Alaskan earthquake (Haas et al. 1977, Yasui 2007, Fitch et al. 2010, Aldridge 2011). Both Haas et al. 1977 and Yasui 2007 elaborated on this finding by pointing out that the lesser damaged structures will take less time and resources to complete (Aldridge 2011). They continued to state that the most severely damaged areas will lag in reconstruction due to more resources necessary

for either intricate repairs or complete rebuilds as well as issues of shorter housing supplies for temporary residence (Aldridge 2011). This finding was demonstrated in an economic assessment by Desilva et al. 2004, which inferred recovery based on property values returning to pre-tornado disaster prices in Oklahoma County. They found that the housing prices associated with the most incredibly damaged ranking of an F5 lagged the market prices of less damaged homes before finally rebounding three years later. This illustrates the significance that the magnitude of the biophysical impact has on the rate of recovery (Cutter 1996; 2000; 2003, Fitch et al. 2010).

Within short-term reconstruction, another indirect ramification of the impact to consider is the decision to rebuild or relocate. This decision is predominantly based on the loss of livelihood and income opportunities or fear of another event (Paul 2005). In a study by Paul 2005, he examined the connection between aid and outmigration in of a tornado disaster in north-central Bangladesh. Through mail surveys and interviews, he discovered that all residents stayed based on receiving more aid than anticipated. However, he did point out that the generous amount of aid was in response to a previous tornado disaster in this region that had generated negatively publicity based on government negligence. Contrary to this finding, another study by Cross 2001 revealed that only half of the population returned to the rural community of Spencer, Kansas, Cross (2001) based on mail surveys without mentioning of aid amounts. His study focused more on the rural versus urban argument in which small town livelihoods played a crucial role in the decision to remain and rebuild.

2.2 Damage Assessment

Once a tornado has occurred, damage surveys are conducted to determine the inferred intensity of the tornado and extent of its path. From these surveys, the tornado is assigned an F-scale rating on the Fujita Scale based on correlating inferred wind speeds from the observed degrees of damages (Fujita 1971, 1981, Fujita and Smith 1993, McDonald 2002, Marshall 2002). All observed tornadoes have been assigned an F-scale rating since the implementation of the Fujita Scale in the 1970s and continues to be the most requested statistic following a tornado disaster to date (Grazulis 1991, McCarthy 2003).

Although the Fujita scale is meant to be an intensity scale, this scale is really more of a damage scale (Doswell and Burgess 1988). F-scale ratings implicitly equate damage with intensity primarily based on its interception with the constructed environment (Doswell and Burgess 1988, Brooks 2003, Doswell et al. 2003, Dotzek et al. 2003). Significant tornado ratings, F3 or higher, are often assigned only when tornadoes initiate construction failure and scatter debris over large expanses (Doswell et al. 2003, Dotzek et al. 2003). In relatively remote locations, tornadoes that are observed are usually assigned much lower ratings because their paths often traverse vegetative cover with little chance to intersect infrastructure. Although tornadoes in densely populated regions are more likely to be reported with higher damage ratings, other difficulties exists in rating F-0 tornadoes based on small damage amounts and brief lifetimes (Brooks 2003, Dotzek et al. 2003). These aforementioned problems highlight the issue of the dependency of F-scale ratings with the underline material and not solely on

inferred wind speeds, which this scale aims to achieve (Doswell and Burgess 1988, Doswell et al. 2009).

Additional problems with the Fujita Scale result from the subjective nature in damage assessments and other underline assumptions. When surveying tornado damage, a great deal of uncertainty exists with the interpretation of the single paragraph descriptors that are often deemed vague and limited in scope (Grazulis 1991, Marshall 2002). These biases are often exacerbated based on the knowledge of different estimators, which can lead to spatial and temporal inconsistencies in rating tornadoes (Doswell et al. 2009). Other discrepancies can be attributed to the assumption of well-built structures and their homogeneous construction instead of the considering the construction the variability of construction (Marshall 2002, Doswell et al. 2009). As a result, these problems and inconsistencies can affect the completeness and accuracy of tornado climatology (McCarthy 2003, Doswell et al. 2009).

Some of these issues were addressed with the modification of the Fujita Scale to develop the Enhanced Fujita Scale. Adjustments included more detailed damage descriptors to reduce subjectivity in damage surveys and account for construction variability and building types (Doswell et al. 2009). Additional damage indicators were also implemented to deal with damages to different types of vegetation (Doswell et al. 2009). However, these indicators still fail to represent the various vegetation types as well as capture any of the antecedent conditions in terms of soil saturation that may contribute to damage severity. In addition to the improved damage descriptors, wind speed ranges were also

lowered based on the observation of building failure initiation at much lower speeds than previous thought (Doswell et al. 2009). Yet, despite these modifications, problems still remain due to the inherent subjectivity in damage surveys and dependency of intercepting structures necessary to infer tornadic intensity with wind speeds.

Despite the aforementioned issues in the Fujita Scale, relating damage to intensity can be useful in modeling hazards associated with tornadoes (Schaefer et al. 2002, McCarthy 2003). Since implementing the Fujita Scale, damaged surveys have noted the different magnitudes of observed damages based on rough guidelines built in the scale (Doswell and Burgess 1988). Upon surveying different damage swaths, weaker structures were more susceptible to wind damage based on materials and poor construction practices (Marshall 2002). Within the past decade, damage surveys have brought forth new information on the correlation of structural engineering and quality to observed damages.

In particular, detailed surveys of the Moore, Oklahoma tornado made important discoveries concerning the relationship between architectural design and degrees of damage. Roof attachment and geometry were found to contribute to the magnitude of damage as the result of weight distribution and number of connections (Brooks and Doswell 2002, Marshall 2002). These results were important findings considering structural failure is often initiated when uneven pressure fields expose these connections. Garage doors also posed a higher risk for greater damage since positive wind pressure can easily raise these relatively flimsy doors (Marshall 2002, Brooks and Doswell 2002). This breach of

envelope creates additional pressure side loads that can cause the roof to uplift and often initiates structural failure (Marshall 2002).

In addition to the direct impacts of the tornado itself, indirect impacts such as projectiles or debris can often aggravate the extent of the damage path as well as magnitude. Once a building has been compromised, projectiles in the debris field become a serious threat to surrounding structures especially those downwind (Marshall 2002, Pan et al. 2002). These projectiles can breach the external envelopes of structures that might have otherwise resisted damage. Evidence of this damage pattern can be seen emanating out from the source in a cascading pattern suggesting the presence of vulnerable structures either directly within the path or on the fringe (Brooks and Doswell 2002, Pan 2002).

Valuable information obtained from damage surveys in conjunction with working with the Enhanced Fujita scale could still lead to instituting better mitigation strategies. With any tornado occurrence, wind speeds can vary greatly with the most intense winds often confined to a small area within the path. The actual likelihood of encountering these winds associated with F3 rated tornadoes or higher is relatively low based on the climatology of observed significant tornadoes (Brooks and Doswell 2000, Dotzek et al. 2003). Thereby, structural integrity could be designed to handle most tornadic wind fields (Marshall 2002). Marshall pointed out that "when wind speeds are overestimated in the Fujita Scale, the general public, designers and builders may conclude that is economically unreasonable to design for these higher wind speeds and associated loads (Marshall 2002, p597)." Understanding how engineering improvements can

withstand the majority of tornadic winds could lead to policy changes in building codes and other construction practices, thus aiding those most vulnerable to such disasters.

2.3 Aerial photography

Historically, tornado damage has been measured by ground and aerial surveys. Beginning in 1965, the Fujita group used aerial photography and ground surveys to determine multi-scale airflows of tornadoes and microbursts through damage assessments (Fujita and Smith 1993, Yuan et al. 2002). They found that tornadoes had highly convergent swirling wind patterns that affected a relatively narrow swath (Fujita 1981). These paths were easily discerned in violent tornadoes based on damaged structures and associated debris (Fujita 1981). Aerial photographs captured additional information of blown down grasses, but often lost track of the path associated with weaker tornadoes or tornadoes in dissipating stages (Fujita 1981, Fujita and Smith 1993). Ground surveys alone proved too difficult in distinguishing weak tornadoes and downbursts.

From aerial damage assessment, the Fujita group identified multi-scale surface winds associated with tornadoes and their resulting damage patterns. The multi-scale winds are the mesocyclone, the tornado, and suction vortices, which are one magnitude smaller than the parent tornado. Instead of newly devoid vegetative swaths, it was discovered that suction vortices would pick debris up near its rotational center and deposit it along their axes (Fujita 1971, 1981, Fujita and Smith1993). The level of damage sustained proved to be a function of the relative positioning of objects within its path to suction vortices rotating around

the tornado itself as well as the tornado's diameter and ratio of rotational to translational velocity (Fujita 1981, Fujita and Smith 1993).

While aerial surveys have played a vital role in gaining knowledge of the dynamics and structure of a tornado, this approach does have its limitation. Aerial surveys tend to be time consuming and costly in locating such an operations as well as processing imagery (Yuan et al. 2002, Jedlovec et al. 2006, Myint et al. 2008). Analysts must have prior knowledge of the affected region to capture the damage swaths (Yuan et al. 2002, Jedlovec et al. 2006). Even with this prior knowledge, additional damaged tracks that were not reported could easily go undetected especially in remote regions (Yuan et al. 2002, Speheger et al. 2002, Jedlovec et al. 2006, Myint et al. 2008). In cases of supercell outbreaks, not all tornado tracks may be examined in detail due to limited resources and attention focused on swaths that sustained the most damage (Fujita and Smith 1993).

2.4 Remote Sensing

Remote sensing can help minimize problems associated with traditional methods. With routine satellite acquisition and reduced costs of satellite imagery, damage assessment can be completed in a relatively inexpensive and timely manner (Yuan et al. 2002, Myint et al. 2008). In addition, satellite data can detect larger swaths of the damage tract provided with the synoptic view (Yuan et al. 2002, Myint et al. 2008). This synoptic view also provides access into otherwise inaccessible regions on the ground from either the debris field or remote locations (Yuan et al. 2002, Jedlovec et al. 2006, Myint et al. 2008). Another advantage of using satellite imagery is the ability to detect damaged areas not discernable to the

human eye through change detection methods and other geospatial techniques (Yuan et al. 2002, Jedlovec et al. 2006, Myint et al. 2008).

Change detection methods have been widely utilized in monitoring land cover changes either anthropogenically induced or disaster-related (Singh 1989, Jensen 1996). These techniques have been employed in many large-scale disasters such as earthquakes (Rejaie and Shinozuka 2004, Sun and Okubu 2004), hurricanes (Wang et al. 2010, Kelmas 2009, Heneka and Ruck 2008, Lee et al. 2008), tsunamis (Belward et al. 2007, Kaplan 2009), wildfires (Gitas et al. 2008), landslides (Lin et al. 2004) and floods (Wang et al. 2002, Islam and Sado 2000) and a few small-scale disasters such as hail (Bentley et al. 2002) and tornado assessments (Yuan et al. 2002, Jedlovec et al. 2006, Myint et al. 2008, Myint et al. 2008b).

The most common approach employed for hazard analyses has been multi-temporal differencing of imagery with the same sensor properties and resolution size. In this method, pixel values assigned in the pre-event image are subtracted from pixel values of the post-event image creating a changed image (Singh 1989, Bentley 2002, Lillesand et al. 2004). Alterations in surface features can then be discerned based on changes in surface orientation or reflective properties as a result of the disaster (Bentley et al. 2002, Yuan et al. 2002, Jedlovec et al. 2006, Myint et al. 2008).

Band-ratio techniques in conjunction with multitemporal differencing often yield better results in capturing changes associated with natural disasters. Band ratio techniques manipulate the data contained in the multispectral bands

into indexed values by aggregating spectral responses of similar class features (Sabins 1997, Lillesand et al. 2004). Working with known indexed values not only makes it easier to track changes with different land class types, but can also minimize scene differences by removing atmospheric effects (Yuan et al. 2002, Lillesand et al. 2004, Jedlovec et al. 2006). While the resulting indexed images can be used as stand-alone composites for direct comparison, multitemporal differencing of these indexed images are often more effective in detecting the smallest changes that could often go unnoticed (Yuan et al 2002).

Normalized Difference Vegetation Index (NDVI) is the most popular index used in damage assessments and recovery analyses (Lin et al. 2004). NDVI has been extensively employed to assess vegetative health, but can also indicate the type of changes in other land classes based on known indexed values (Rouse et al. 1973, Yuan et al. 2002, Lin et al. 2004, Jedlovec et al. 2006, Wilkinson and Crosby 2010, Roemer et al. 2011).

In studies by Yuan et al. 2002, Jedlovec et al. 2006, and Myint et al. 2008, they used NDVI composites as part of their damage assessment of a tornado disaster. They found that NDVI composites not only captured a broader portion of the tornado track, but could also differentiate between soil deposition and vegetation removal from tornadic winds. Yuan et al. 2002 found that NDVI composites could discern F2 related damages in the urban affected regions and F3 damages in the rural areas of their analysis. Bentley et al. 2002 also discovered that NDVI could distinguish between hail and wind damage in their severe storm damage assessment. They revealed that hail damage vegetation had significantly

lower NDVI values as the crop was completely destroyed, whereas wind damaged vegetation had relatively minor differences in NDVI values due to only temporary disruptions in photosynthesis.

Even though NDVI composites have obtained valuable information in disaster analysis, NDVI differencing has illustrated more success at discerning damages and reconstruction. Yuan et al. 2002 was able to detect more portions of the tornado track using NDVI differencing than NDVI composites with F2 damages captured in the rural areas and some F1 damages detected in urban regions. They also demonstrated that NDVI differencing could delineate between F-scale damages based on decreasing values with increasing F-scale ratings using overlay analysis of F-scale damage data. Wilkinson and Crosby (2010) also linked NDVI differencing values to tornado damage. However, unlike Yuan et al. 2002, their study was more simplistic in that they classified NDVI differenced values into categories of light, moderate and severe damages.

NDVI and NDVI differencing does, however, have some problems in providing a complete damage survey. First, monitoring vegetative damage tends to be difficult using NDVI as stated by Bentley et al. 2002, because vegetation is often blown and not uprooted in grassland or agriculture crop regions. With these ground covers, much of the vegetation survives resulting in only subtle changes in NDVI values making it difficult to detect any changes (Bentley et al. 2002, Jedlovec et al. 2006). Other pitfalls with NDVI scenes correspond to seasonal differences in vegetation and climatic changes that could complicate damage assessments (Bentley et al. 2002, Yuan et al. 2002, Jedlovec et al. 2006, Myint et

al. 2008). Jedlovec et al. 2006, in particular, noted problems due to spring greenness that degraded the track's signal in urban settings. NDVI also begins to fail in detecting portions of the tracks along rivers and other water bodies possibly due to similar reflectance values between bare soil of the tornado track and riverbanks (Jedlovec et al. 2006, Yuan et al. 2002). Additionally, Jedlovec et al. 2006 reported some signature confusion between exogenous land use changes due to a newly constructed road and land degradation from the tornado based on very similar NDVI values.

Other spectral enhancements such as principal component analysis (PCA) can be helpful in detecting damaged pixels in urban areas despite some of their problems. Yuan et al. 2002 found that depending on the channels used to collect data, PCA could extract some damage information in urban areas by reducing noise and scattering associated with the atmosphere (Yuan et al. 2002). Myint et al. 2008 also found PCA effective in discerning the damaged path due to the contrasting signatures of vegetation and soil surfaces. However, Jedlovec et al. 2006 noted difficulties with PCA detecting damage in rural environments where land cover is fairly homogeneous due to subtle changes in texture. PCA also has trouble recognizing the damage tract in severe damage cases where debris has been scattered into small fragments (Jedlovec et al. 2006).

Classification techniques in conjunction with spectral enhancements have also been utilized in many disaster studies including tornado damage assessments. These techniques have been frequently used to differentiate between damaged and non-damaged regions (Chou et al. 2009). More recently, shifts from pixel-based

approaches to object-oriented approaches have significantly improved their degree of accuracy increasing their popularity in hazard analysis (Myint et al. 2008b, Wentz et al. 2009).

Myint et al. 2008 demonstrated this finding with their damage assessment of the 1999 Moore, Oklahoma tornado. Using PC3 and PC4, they classified damaged and non-damaged portions of the track using both traditional methods of supervised and unsupervised approaches and object-oriented approach. His study highlighted problems with traditional classification methods due to the high variability in urban settings that matched the chaotic pattern of fragmented debris. By developing an effective algorithm tailored to spatial relationships of segmented objects in terms of damaged and non-damaged regions, they found the highest accuracies using object-oriented approach over the traditional pixel-based techniques. However, despite this improvement, their study still had problems in detecting some of the fine scale damages associated with F0 and F1 ratings near the river proving the difficulty in discerning small-scale damages.

Other geospatial-based research has used spatial indexes as a means to capture damaged regions. Myint et al. 2008b performed such an analysis on the same tornado to identify the different F-scale damages within the track. They were able to correlate the changing spatial arrangements of objects with the different magnitude of damages using Getis Index and a window size of 21X21. Although their study had some problems identifying some of the F-scale damages due to resolution size, this method could still serve as an alternative to ground studies where accessibility is a concern and fine resolution imagery is available.

From these tornado damage assessments, factors of land cover classes, damage severity and image quality should be considered when selecting spectral enhancement type and imagery for future research. The ability to detect tornado damage depends on the underline land cover and damage severity as noted by Yuan et al. 2002, Jedlovec et al. 2006, and Myint et al. 2008. Urban areas with high-class variability often obscure the track because of the similar chaotic pattern in the tornado (Yuan et al. 2002, Myint et al. 2008). While homogeneous regions such as forested regions were overall easier to discern, some vegetative covers are problematic based on texture, land cover type and damage magnitude (Yuan et al. 2002, Jedlovec et al. 2006). Additionally, image quality plays a key role in the ability to discern damaged regions as Jedlovec et al. 2006 study was plagued with atmospheric contamination from evaporation of damp surfaces and selection of coarse resolution (250 meters). These issues can hamper the ability to discern the damage track (Myint et al. 2008,Yuan et al. 2002).

While the aforementioned studies only employed remote sensing techniques for tornado damage assessments, other analyses have used geospatial methods to examine the recovery process from large-scale disasters. These studies have obtained valuable in recovery by investigating uncovered spatial disparities that could be applied in reconstruction assessments of small-scale events such as tornadoes. One such example is Lin et al. 2004 study of an earthquake-induced landslide in Central Taiwan. Using a recovery index and NDVI differenced images, their study assessed vegetation restoration of landslide-affected region. Their analysis was able to distinguish between damaged and

recovered regions and establish recovery rates based on the resulting index values. By classifying recovery rates into ordinal rankings, they were also able to investigate the spatial disparities in recovery where they uncovered further land degradation after the landslide in the steep sloped areas.

In a similar recovery analysis of a different landslide-damaged area, Chou et al. 2009 employed a modified version of Lin et al. 2004 recovery index using an exponential derivative. In their study, they predefined the damaged regions first using unsupervised classification techniques using weighted values and then employed their index. Although their index correlated recovery with low index values unlike Lin et al. 2004, they too uncovered vulnerable regions in vegetation regeneration along the river due to escarpment and invasion of non-native species. As a result of this finding, they also noted that complete recovery was never attained during their six year analysis.

Another recovery study conducted by Roemer et al. 2011 examined the recovery rates for a tsunami-affected area. They also modified Lin et al. 2004 index, but used the same recovery rate values as Lin et al. 2004 unlike Chou et al. 2009. They defined the damaged area like Chou et al. 2009, but employed an impact threshold based on statistically analysis of sampled pixels to capture the impacted region. Using this approach, they could distinguish between recovered and damaged regions for each subsequent recovery analyzed. Through classification accuracy assessments, their results proved successful when compared with ground truth data with overall accuracies of 80.77%. From their

results, they also revealed disparities in recovery rates due to different vegetative species and shoreline exposure similar to Chou et al. 2009 findings.

Roemer et al. 2011 also used change vector analysis (CVA) as a means to cross-reference his recovery index results. By detecting positional changes in damaged and recovered pixels, their study could further investigate into the type of land use changes after the tsunami and rate of recovery (Roemer et al. 2011, Wang et al. 2009, Lunetta and Elvidge 1998, Engvall et al. 1977). By linking different vegetation species data, they noted high recovery rates with non-woody plants such as grasslands and low recovery rates for woody species. They also discovered through CVA that human induced land use changes could have contributed to low recovery rates in certain sections.

2.5 Conclusion

Hazard studies have uncovered many facets to disasters concerning the initial impact and recovery process. These variables include both the biophysical impact and social vulnerabilities. Much of this research has focused on recovery from large-scale events in terms of hurricanes, tsunamis, floods and earthquakes with few studies examining the reconstruction after a tornado disaster. These few hazard studies have primarily focused on recovery from an economic assessment using county assessor data or outmigration studies employing qualitative methods.

More recently, remote sensing methods have been used in damage assessment of the biophysical impact of a tornado, but have yet to be employed in recovery assessments of this hazard type. Large-scale disasters have examined both aspects of hazards from the initial impact and reconstruction analyses.

Therefore, the need still exists to provide an objective view of the reconstruction from a tornado disaster and understand the rate of recovery as a function of the biophysical impact from a hazard perspective.

3. Study, Data and Methods

3.1 Introduction

Remote sensing has demonstrated to be a valuable tool in monitoring land changes as a result of anthropogenic change or natural disasters (Mura et al. 2008). Most disaster research that utilizes remote sensing has focused on large-scale disasters such as earthquakes (Rejaie and Shinozuka 2004, Sun and Okubu 2004), hurricanes (Wang et al. 2010, Kelmas 2009, Heneka and Ruck 2008, Lee et al. 2008), tsunamis (Belward et al. 2007, Kaplan 2009), wildfires (Gitas et al. 2008), landslides (Lin et al. 2004) and floods (Wang et al. 2002, Islam and Sado 2000)), while only few studies have analyzed small-scale disasters like the aftermath of a tornado. The few tornado studies (Myint et al. 2008, Myint et al. 2008b, Jedlovec et al. 2006, Yuan et al. 2002, Wilkinson and Crosby 2010) have focused on the initial impact from a damage assessment perspective. Consequently, the need to examine reconstruction for even small-scale disasters like tornadoes still exists. The fundamental goal of this research attempts to fill that void by examining reconstruction from a tornado disaster through remotely sensed data and a series of image processing algorithms. This chapter discusses the study area for the research, data and methods employed in the analysis.

3.2 Study Area

This research examines a tornado disaster in Central Oklahoma located in the Southern Great Plains. This region sits within the Mississippi River basin where rich soils and proximity to the Canadian River provide fertile land for agricultural purposes. With a mixture of rural and urban landscapes, this stretch

of Oklahoma includes the state capital, Oklahoma City, as well as the smaller cities of Newcastle, Moore, Norman and Bridge Creek. The climate in this region has a mean annual temperature of 60 degrees Fahrenheit with seasonal temperature extremes that vary below 32 degrees Fahrenheit in the winter to above 90 degrees Fahrenheit in the summer (OCS 2010). Mean annual precipitation averages to 42 inches per year, but can deviate significantly according to the seasons (OCS 2010). Most notably, the relatively flat terrain allows for the formation of some of the worst convective storms during the springtime and late fall when warm tropical air masses from the south clashes with the dry, polar air to the north (Bluestein 2006, Grazulis 1991). As a result of this synoptic climatology, a high frequency of tornadoes is produced per year, thus earning its nickname of Tornado Alley (Bluestein 2006, Grazulis 1991).

Within Central Oklahoma, this study concentrates on the reconstruction of tornado track A9 shown in Figure 1. Out of 74 tornadoes spawned from the May 3, 1999 supercell outbreak, track A9 was the most significant tornado producing devastating damages associated with an F5 rating (refer to Chapter 2 for information on the Fujita Scale) in the cities of Moore and Bridge Creek (Speheger et al. 2001). This tornado touched down in the central part of Grady County near the town of Amber and traveled northeast for 38 miles through the cities of Moore and Bridge Creek and dissipated on the eastern side of Oklahoma City in Oklahoma County. While it could be argued that the two tornado tracks A6 and A8 southwest of Chickasha could be a discontinuity of the focused track, the NOAA's publication "Storm Data" records each touchdown as a separate

tornado (NCDC 2010). Therefore, this research only examines the continuous track labeled A9.

This particular tornado serves as a good example for analyzing the reconstruction process of a tornado disaster because of its track length, path and varying degrees of damages. This tornado tracked 38 miles on the ground, which is considered a very long track compared to other recorded tornadoes (NCDC 2010). While on the ground, the tornado traversed different land cover types affecting both rural and urban areas. Within its path, the magnitudes of damages varied significantly thus affecting its Fujita Scale ratings from moderate damages of an F1 rating to the incredible damages of an F5 rating (Fujita 1971, 1973, 1981). With such a diverse cross-section of factors involved, this tornado disaster provides a rare opportunity to monitor recovery.

This study examines the recovery process of the Moore, Oklahoma tornado for 2000, 2001 and 2002 by employing geospatial techniques with remotely sensed data. These data are detailed in the next section along with F-scale data provided by the Oklahoma Weather Center. Following the data section, the methodology portion is discussed in which two change detection methods are presented to evaluate reconstruction. The first method quantifies recovery through a series of image processing algorithms with a set of spectrally enhanced images. The second method uses change vector analysis as a means to qualitatively assess reconstruction.

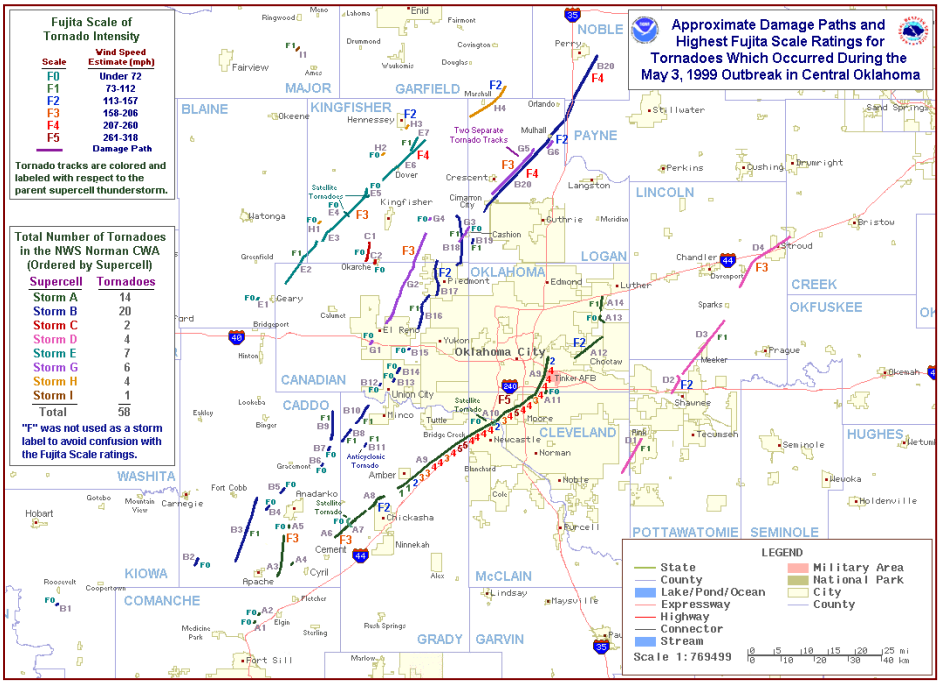

Fig. 1. Map of recorded tornado locations during the May 3, 1999 Tornado Outbreak in Central Oklahoma. (image from http://www.srh.noaa.gov/images/oun/wxevents/19990503/maps/bigoutbreak.gif)

3.3. Data and Data Preparation

For this multitemporal study, reconstruction was assessed using both Landsat Thematic Mapper (TM) and Landsat Enhanced Thematic Mapper (ETM+) imagery at 30 meter spatial resolution with seven multispectral channels spanning the blue to thermal portions of the electromagnetic spectrum. All of the multispectral bands were utilized except for the thermal band due to its coarse resolution (Myint et al. 2008). The panchromatic band was also excluded as a result of its availability only with Landsat ETM+ data as well as its finer spatial resolution than all the other bands. Cloud-free imagery for Central Oklahoma (path 28, row 35) were obtained prior to the tornado disaster on June 26, 1998 and

after the disaster on May 12, 1999, May 30, 2000, April 23, 2001 and September 17, 2002 listed in Table 1. Ideally, imagery should be collected within two weeks of the anniversary date for each scene, however, cloud contamination proved problematic (Singh 1989, Jensen et al. 1995, Lillesand et al. 2004). Therefore, the scenes for 1998 and 2002 were selected based on similar vegetative greenness to ensure successful change detection analysis (Mahiny et al. 2007). Images after 2002 were not collected due to the lack of cloud-free scenes prior to the occurrence of another tornado within the study area on May 8, 2003.

Table 1. Specific satellite imagery utilized in the study

Date	Satellite	Spatial Resolution
June 26, 1998	Landsat TM	28.5 meters
May 12, 1999	Landsat TM	28.5 meters
May 30, 2000	Landsat TM	28.5 meters
April 23, 2001	Landsat ETM+	28.5 meters
September 17, 2002	Landsat ETM+	28.5 meters

The selected scenes were pre-processed to reliably monitor changes attributed to the recovery process (Townsend et al. 1992). To minimize distortion of actual surface reflectance from haze, relative radiometric corrections were performed using the Cos(t) model in IDRISI Taiga (Version 16). This process removes artifacts due to solar illumination, atmospheric scattering and absorption by subtracting digital numbers of dark objects (deep-water bodies or shadows) that should have pixel values close to zero (Chavez 1988, 1996, Mahiny et al. 2007). However, due to the absence of a dark object in the scene, histogram thresholds representative of haze were used. These values were located by sharp increases in the histogram and then subtracted from each band (Chavez 1996). Digital numbers were converted to apparent reflectance and imported into Erdas Imagine 9.3 for further pre-processing and analysis.

To ensure successful change detection of the tornado disaster, post-tornado imagery were co-registered and normalized (Mahiny et al. 2007). Post-tornado images were co-registered to the pre-tornado image below the standard root mean square error (RMSE) of 0.5 pixels to minimize pixel misregistration (Myint et al. 2008b). Although locational errors cannot be entirely eliminated, this procedure significantly reduces anomalous results attributed to spatial inconsistencies (Myint et al. 2008b, Myint and Wang 2006, Townsend et al. 1992). After co-registration, post-tornado scenes were normalized based on densely vegetative values in the pre-tornado image to reduce reflectance variations between the imagery (Mahiny et al. 2007, Hall et al. 1991, Jensen et al. 1995, Lunetta and Elvidge 1998). Band values for each image were adjusted as needed by adding the difference of these averaged reflectance values between the selected post-tornado image and pre-tornado image to the selected post-tornado image (Hansen et al. 2008).

After pre-processing the data to obtain corrected surface reflectance values, each image was layer stacked and subsets were made to extract the tornado-affected region. This region covered 1689.62 km^2 with upper left coordinates of longitude 97° 44' 36.537" W and latitude 35° 35' 32.057" N and lower right coordinates of longitude 97° 19' 4.331" W and latitude 35° 12' 0.343" N. An example of a corrected image of the study area is referenced in Figure 2 and shown in Figure 3 as a false color composite displaying Bands 4, 3 and 2 as red, green and blue respectively.

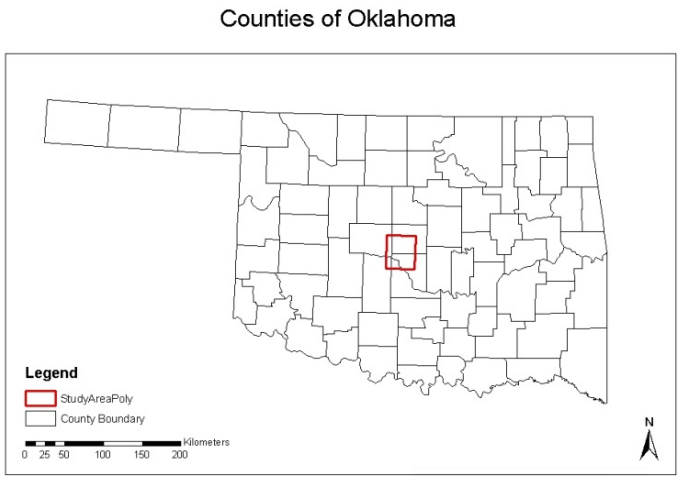

Fig. 2. Map displaying county boundaries in the state of Oklahoma and the study area outlined in red.

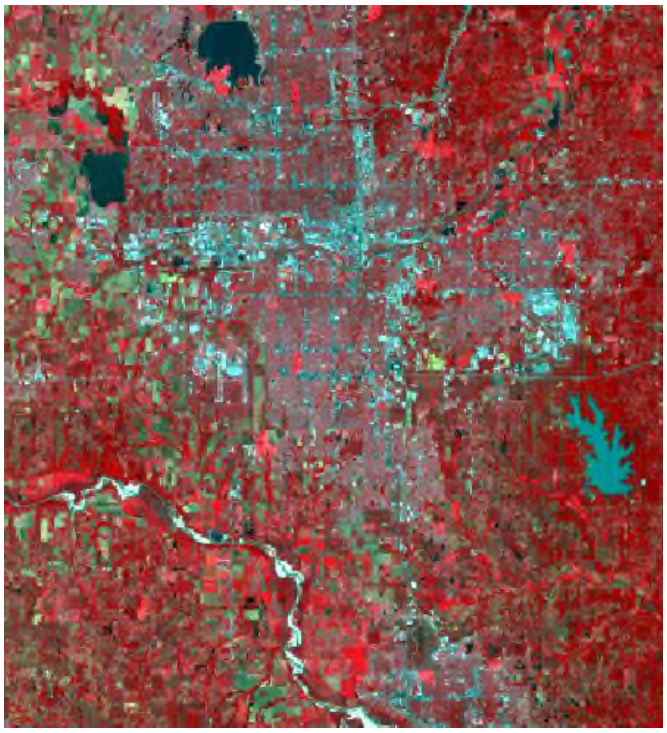

Fig. 3. False Color Composite of the Study Area displaying Band 4 in red, Band 3 in green and Band 2 in blue.

In conjunction with Landsat imagery, F-scale contours developed from the Oklahoma Weather Center were utilized to define the exact damage track (Yuan et al. 2002, Speheger et al. 2002). Using a high resolution F-scale map provided by Speheger et al. 2001, F-scale contours were digitized in ArcGIS 9.3. These contours were geo-referenced in Universal Transverse Mercator projection Zone 14 with World Geodetic System 1984 spheroid using the United States Geological Survey Quadrangles, Oklahoma City North and Oklahoma City South, at a scale of 1:100,000. The resulting shapefile was then clipped to the post-tornado image to exclude a small portion of the track that extended into the adjacent scene below. This decision to omit less than 10 miles of the track in a predominantly densely, vegetative region was based on the requirement of radiometric normalization. Including the adjacent scene would require different radiometric corrections tailored to each scene for each year. This would have more than likely complicated results by introducing errors, therefore this scene and segment of track was not included in the analysis. The final F-scale shapefile was transformed into an Area of Interest file (AOI) using the perimeter of the entire damaged track to extract recovery information for all the F-scale zones.

3.4. Digital Analysis

In order to monitor reconstruction of the Moore, Oklahoma tornado, spectral enhancements were performed using data transformations and indices. Both enhancements manipulate the original multispectral bands to create a new image that can highlight alterations in land cover associated with the tornado (Yuan et al. 2002). Data transformations typically generate more meaningful

images by reducing data redundancy, while indices use band ratios in order to aggregate land cover types based on similar spectral responses (Singh and Harrison 1985, Yuan et al. 2002). Indices, in particular, could prove instrumental in assessing recovery based on the premise that alterations in surface features are correlated with changing index values (Yuan et al. 2002, Bentley et al. 2002, Myint et al. 2008).

Spectral enhancements based on data transformations were generated for damage and reconstruction assessment using tasseled cap transformations. This transformation type manipulates the six bands into six new composite bands. TCT enhances the structures in scene classes based on weights with the most useful information usually captured into the first three bands brightness (Sabins 1997, Jensen et al. 1995, Lillesand et al. 2004). The set of equations for the first three TC bands equation is listed below:

$$\begin{aligned} TC1 = {} & 0.307(TM1) + 0.2793(TM2) + 0.4743(TM3) + 0.5585(TM4) \\ & + 0.5082(TM5) + 0.1863(TM7) \end{aligned} \tag{3.1}$$

$$\begin{aligned} TC2 = {} & 0.2848(TM1) + 0.2435(TM2) + 0.5436(TM3) + 0.7243(TM4) \\ & + 0.0840(TM5) + 0.1800(TM7) \end{aligned} \tag{3.2}$$

$$\begin{aligned} TC3 = {} & 0.1509(TM1) + 0.1973(TM2) + 0.3279(TM3) + 0.3406(TM4) \\ & + 0.7112(TM5) + 0.4572(TM7) \end{aligned} \tag{3.3}$$

where (TC 1), greenness (TC 2) and wetness (TC 3) respectively measure soil brightness, vegetative greenness, and soil moisture and canopy (Kauth and Thomas 1976, Crist and Cicone 1984, Crist 1985). This type of imagery could

help discriminate between damaged and recovered land covers by transforming the original image into a more meaningful interpretation (Yuan et al. 2002).

In addition to Tasseled Cap transformations, spectral enhancements of vegetative and urban indices as well as a combined index of these two components were generated to help evaluate the recovery process. The first vegetative index, Normalized Difference Vegetation Index (NDVI), has been extensively used to monitor vegetative health as well as distinguish between different land cover types (Rouse et al. 1973, Bentley et al. 2002, Yuan et al. 2002, Roemer et al. 2011). This index quantifies the spectral signatures of ground features using the near-infrared (NIR) and red (R) bands on a scale of -1.0 to +1.0 according to the following equation:

$$\mathrm{NDVI} = \frac{\mathrm{NIR(Band4)} - \mathrm{R(Band3)}}{\mathrm{NIR(Band4)} + \mathrm{R(Band3)}} \tag{3.4}$$

(Tucker 1979, Jackson et al. 1983, Marsh et al. 1992, Yuan et al. 2002). Index values fall in the high positive range for vegetation, low positive for artificial surfaces, negative values for water features and near zero for bare soils (Rouse et al. 1973, Bentley et al. 2002, Yuan et al. 2002, Roemer et al. 2011, Villa 2007). By understanding the range of values associated with vegetative health and land cover types, land cover changes associated with the Moore, Oklahoma tornado can be monitored based on changing NDVI values (Yuan et al. 2002). Therefore, NDVI outputs were generated for 1998, 1999, 2000, 2001 and 2002 to assess recovery.

Another popular vegetative index utilized in this analysis is the Soil Adjusted Vegetative Index (SAVI). This index uses the same-scaled values as

NDVI based on the manipulation of the same bands. However, SAVI differs from NDVI by using a soil correction factor (L) in the following equation:

$$SAVI = (1 + L)\frac{NIR(Band4) - R(Band3)}{NIR(Band4) + R(Band3) + L} \quad (3.5)$$

where L ranges from 0 to 1. This factor minimizes the external effects from solar irradiances variations due to atmospheric effects or the interaction of spectral responses between canopy cover and soil brightness (Huete 1988, Gilabert et al. 2002, Villa 2007). Therefore, SAVI images were generated for each year using the standard soil correction factor of 0.5, since exact soil conditions were unknown (Huete 1988).

In addition to vegetative index outputs, Urban Index (UI) images were produced to aid in recovery assessment especially in urbanized areas. This index can highlight damages to built-up areas such as buildings, asphalt and other impervious surfaces by incorporating information obtained in the second mid-infrared band (MIR) and near-infrared band (NIR) using the following equation (Kawamura et al. 1997):

$$UI = \frac{MIR(Band7) - NIR(Band4)}{MIR(Band7) + NIR(Band4)} \quad (3.6)$$

The Urban Index has the same range as the aforementioned indices, but differs from the vegetative indices by assigning high positive values to artificial surfaces and low negative values to vegetative surfaces (Kawamura et al. 1997, Villa 2007). With such a wide range between vegetative and man-made surfaces, this index could potentially better evaluate the recovery process in residential areas and other built-environments.

I also explored two new indices that I believe could be better suited for monitoring the effects of natural disasters such as the Moore, Oklahoma tornado. The first index merges the Urban Index and NDVI into what I call the Combined Vegetative Urban Index (CVUI) by combining the red (R), near-infrared (NIR) and second mid-infrared (MIR) bands using the following equation:

$$\text{CVUI} = \left(\frac{\text{MIR(Band7)} - \text{NIR(Band4)}}{\text{MIR(Band7)} + \text{NIR(Band4)}} \right) * \left(\frac{\text{NIR(Band4)} - \text{R(Band3)}}{\text{NIR(Band4)} + \text{R(Band3)}} \right) \qquad (3.7)$$

By employing these band combinations, the aim of this index is to successfully capture damaged regions in both vegetative and urban land covers based on their sensitivity to the spectral responses of these materials. The second index named the Shortwave Infrared Index (SWIRI) also contains a vegetative assessment component using the near-infrared band (NIR) and first mid-infrared band (MIR) shown in the following equation:

$$\text{SWIRI} = \frac{\text{MIR(Band5)} - \text{NIR(Band4)}}{\text{MIR(Band5)} + \text{NIR(Band4)}} \qquad \text{(Eq 3.8)}$$

With the inclusion of the first mid-infrared band commonly used to delineate moisture content in vegetation and soils, this index could help indicate the state of surface features in terms of damaged and recovered (Sabins 1997). As a result, both SWIRI and the Combo Index could be more effective than the aforementioned indices. Therefore, CVUI and SWIRI images were produced for each year to be included in the analysis.

Using the indexed images (NDVI, SAVI, UI, SWIRI and CVUI), the first change detection method assessed recovery for the years of 2000, 2001, and 2002

utilizing a recovery equation in conjunction with a series of image processing algorithms. This equation was modified from Roemer et al 2011:

$$R = \frac{(\text{Index}_2 - \text{Index}_1) + 2}{(\text{Index}_1 - \text{Index}_0) + 2} \tag{3.9}$$

where R is recovery and Index_2, Index_1 and Index_0 are respectively the images for the recovery year, post-tornado year and pre-tornado year. These indexed images were subtracted according to the aforementioned equation and rescaled using a factor of two changing the possible range from -2.0 to +2.0 to a range of 0.0 to +4.0. While Roemer et al. 2011 respectively employed an impact threshold to define damage as well as overcome a computer algorithm problem of near zero values in the denominator, this study found it necessary to rescale the data instead. This process ensured the inclusion of minor to moderately damaged areas associated with F0 and F1 ratings that could have otherwise been excluded with an impact threshold. After rescaling the data, the resulting images were divided accordingly for each spectral enhancement (index) to produce recovery images for the years of 2000, 2001 and 2002.

These recovery images were further evaluated to capture true recovery by employing different statistical thresholds to account for minor deviations that can occur with annual changes. Using the recovery image for the year 2000, three possible outcomes were generated based on thresholds of 0.5, 1.0 and 1.5 standard deviations from the mean of the entire recovery scene (see Table 2). Values that fell within the selected standard deviation were classified as recovered while out of bound pixels were classified as still damaged. To capture only those pixels that

recovered in the subsequent year, a mask was applied to the 2001 recovery image following the above procedures. This analysis was repeated for the 2002 recovery image using masks for the recovered pixels in 2000 and 2001 to acquire recovery for 2002. This process was repeated for each threshold and spectral enhancement (NDVI, SAVI, UI, SWIRI, and CVUI) yielding a total 45 possible recovery outcomes. Subsets of these images were made to extract recovery information only for the tornado-affected region using the damaged track Area of Interest (AOI) file.

Table 2. List of Threshold Values of 0.5, 1.0, 1.5 standard deviations to define recovery for each spectral enhancement type (e.g. index) and year.

			0.5		1.0		1.5	
Index	Year	Mean	Min	Max	Min	Max	Min	Max
NDVI	2000	1.015	0.987	1.044	0.958	1.072	0.930	1.101
	2001	1.022	0.977	1.068	0.931	1.113	0.886	1.159
	2002	1.000	0.968	1.033	0.935	1.065	0.903	1.098
SAVI	2000	1.009	0.991	1.028	0.972	1.046	0.954	1.065
	2001	1.016	0.986	1.046	0.956	1.076	0.926	1.106
	2002	1.006	0.984	1.028	0.962	1.050	0.940	1.072
UI	2000	0.985	0.951	1.019	0.917	1.053	0.883	1.087
	2001	1.007	0.961	1.054	0.914	1.100	0.868	1.147
	2002	0.996	0.958	1.034	0.920	1.072	0.882	1.110
SWIRI	2000	0.985	0.961	1.009	0.937	1.033	0.913	1.057
	2001	1.010	0.973	1.047	0.936	1.084	0.899	1.121
	2002	1.028	1.000	1.057	0.971	1.085	0.943	1.114
CVUI	2000	0.989	0.965	1.013	0.941	1.037	0.917	1.061
	2001	1.002	0.966	1.039	0.929	1.075	0.893	1.112
	2002	1.005	0.978	1.033	0.950	1.060	0.923	1.088

To compare the results of the recovery outcomes, accuracy assessments were performed and analyzed for each recovery scene. As suggested by Congalton (1991), the minimum 50 points per class (recovered and still damaged) were collected using a stratified random sampling approach generating a total of 100 points per scene (Myint et al. 2008c, Myint 2006, Congalton and Green

1999). The results of these accuracy assessments generated error matrices, which list the overall accuracies, producer's accuracies, user's accuracies and kappa coefficients. These accuracies were averaged according to each threshold and spectral enhancement type and ranked to determine the combination.

The best results were selected to generate maps displaying the annual recovery changes and calculate recovery rates. By overlaying recovery changes for 2000, 2001 and 2002, reconstruction maps were produced to display the annual recovered and damaged regions onto a single map. Annual recovery rates were calculated using the following equation:

$$\text{Recovery Rate} = \left[\frac{\text{Recovery area}}{\text{Total Area}} \right] * 100 \tag{3.10}$$

to assess the total area recovered for each year. F-scale recovery rates were also determined for each F-scale damaged zone by overlaying the F-scale contours onto the reconstruction maps and calculated using the aforementioned equation.

3.5 Change Vector Analysis

The second change detection method, Change Vector Analysis (CVA), was employed in this analysis to help qualitatively assess land use changes in the recovery process. This method examines positional changes in pixels within a two-dimensional space through vector analysis (Roemer et al. 2011, Lunetta and Elvidege 1998, Engvall et al. 1977). The magnitude and directional changes are calculated using the following set of equations:

$$M = \sqrt{\left((ya - yb)^2 + (xa - xb)^2 \right)} \tag{3.11}$$

$$DIR = \tan^{-1}\left[\frac{xa - xb}{ya - yb}\right] \quad (3.12)$$

where M is magnitude, ya and xa are selected bands from the earlier scene and yb and xb are the second set of bands from the latter scene (Roemer et al. 2011, Lunetta and Elvidege 1998, Engvall et al. 1977). The directional changes (DIR) indicate the type of changes within the feature space where 0 to 90 degrees (180 to 270 degrees) correlates with an increase (decrease) in both band values and 90 to 180 degrees (270 to 360 degrees) exhibits an increase (decrease) in band b and decrease (increase) in band a (Roemer et al. 2011, Lunetta and Elvidege 1998, Engvall et al. 1977). By understanding these positional changes, both quantitative and qualitative changes can be attributed to the type and degree of land use changes (Roemer et al. 2011, Engvall et al. 1977). Therefore, change vector analysis was performed using Tasseled Cap transformations employing the greenness (y) and brightness (x) bands respectively.

3.6 Conclusion

In order to examine the reconstruction of the Moore, Oklahoma tornado, remotely sensed data and a series of image processing algorithms were employed. Landsat TM and Landsat ETM+ imagery were acquired for the pre-tornado year(1998), impacted year(1999), and three years after the tornado (2000, 2001, and 2002). These images were pre-processed and normalized to remove artifacts from haze or sun illumination effects and minimize scene variations. In addition to imagery, detailed F-scale data was transformed into a shapefile and clipped to remove a small portion of the track that ran into the adjacent scene. A series of image processing algorithms were utilized to calculate recovery by employing a

recovery index and different thresholds. Classification accuracy assessments were then performed to determine the best transformation type and threshold. With the six top-performing results, both annual and F-scale recovery rates were calculated for each F-scale damaged zone. The results of this analysis are detailed in the following chapter.

4. Results

4.1 Introduction

This research examines the recovery of a tornado disaster using satellite imagery and change detection analysis to investigate whether or not reconstruction is a function of the level of damaged sustained as measured by the Fujita Scale. As previously mentioned, recovery from the Moore, Oklahoma tornado was assessed for the years of 2000, 2001 and 2002 using a series of spectrally enhanced images focusing on vegetation (NDVI, SAVI), urban (UI, SWIRI) and a combination of the two (CVUI) and determined based on different thresholds. From the aforementioned analysis, the top performing results were used to derive annual recovery rates and recovery rates corresponding to each F-scale zone from maps depicting reconstruction. This chapter details the outputs from the recovery index and their overall performances and discusses the trends in the reconstruction maps and both annual and F-scale recovery rates.

4.2 Assessment of New Indices and Initial Impact of Tornado

Before assessing the initial impact or reconstruction of the tornado disaster, the behavior of the two new indices, Shortwave Infrared Index (SWIRI) and Coupled Vegetation and Urban Index (CVUI), were investigated by sampling different land use and land cover types and comparing their values with known indices' values. Based on the sample means of the different land classes listed in Table 3 and shown in Fig.4, both the SWIR and CVUI indices exhibit similar values to UI producing low positive values for bare soil and fallow agriculture and low negative values for healthy vegetation. This pattern is even more evident

in Figure 5 as both SWIRI and CVUI show positive correlations with the UI curve and negative correlations with the SAVI and NDVI curves.

Table 3. Sampled Means of Different Land Cover Classes.

Index	Residential	Commercial	Bare Soil	Fallow Agriculture	Active Agriculture	Dense Vegetation	Water
NDVI	0.462	0.108	0.147	0.202	0.721	0.849	-0.295
SAVI	0.297	0.072	0.121	0.150	0.509	0.502	-0.089
Urban	-0.315	0.027	0.067	0.063	-0.492	-0.662	-0.177
SWIR	-0.148	0.061	0.070	0.132	-0.237	-0.360	-0.128
CVU	-0.156	-0.003	0.007	0.009	-0.366	-0.567	0.053

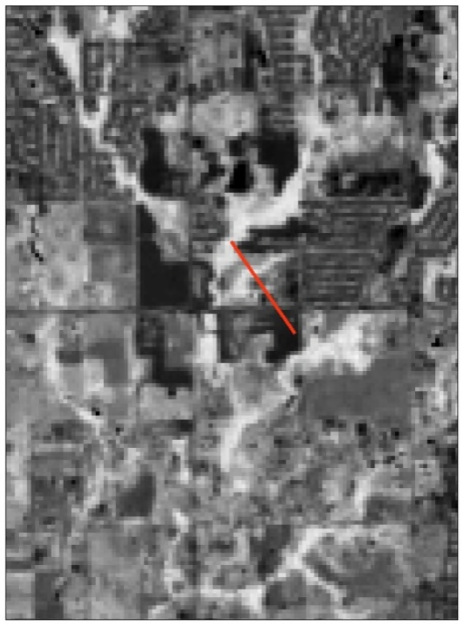

Fig. 4. 1998 Urban Index showing the transect of different land covers of the 1999 Moore, Oklahoma Tornado-impacted region a year before the tornado disaster.

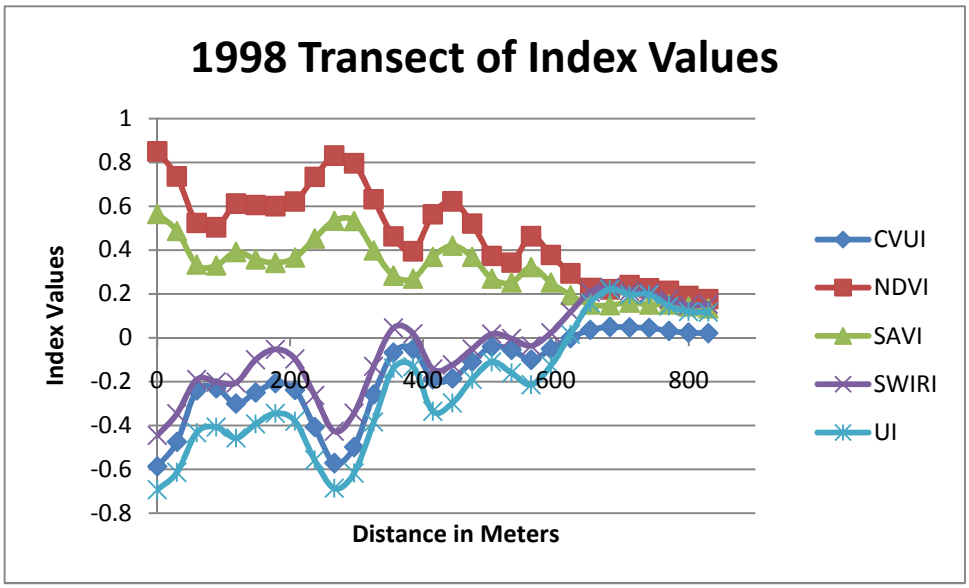

Fig. 5. Reflectance Curves for Coupled Vegetation and Urban Index (CVUI), Normalized Difference Vegetative Index(NDVI), Soil Adjusted Vegetative Index(SAVI), Shortwave Infrared Index(SWIRI), Urban Index (UI) for the Moore Oklahoma tornado-impacted region.

However, SWIRI and CVUI deviate somewhat in terms of their ranges with CVUI values falling in between the lower UI values and higher SWIRI values. The new indices (SWIRI and CVUI) also appear to be less affected by the mixture of vegetation with urban surfaces in the residential areas with overall lower residential values than SAVI, NDVI and UI means.

Both qualitative and quantitative damage assessments revealed that all of the aforementioned indices were able to detect the majority of the damage tract. When visually comparing the post-tornado imagery in Figures 6 – 10, there appears to be no significant differences in discerning the damaged track even with SWIRI and CVUI. Although CVUI captured the same extent of the tornado track, the overall brightness of the scene makes it a little harder to discern the upper

portion of the damaged path within the residential area. Additionally, all of these indices had difficulties in capturing portions of the path near the river as well as the regions of F0/ F1 damages found along the outer edges of the track. However, the F0/ F1 damages could be discerned quantitatively by comparing reflectance curves from the same transect in both pre-tornado and post-tornado imagery (see Figs.4, 5, 11 and 12). These curves illustrate the changes due to the tornado by curve flattening in some sections and near zero values similar to those of bare soil or fallow agriculture indicating scattered debris and damaged vegetation.

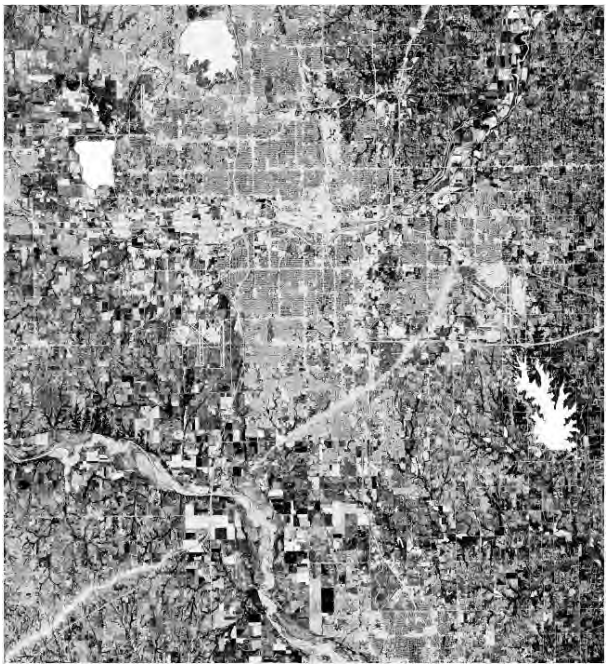

Fig. 6. 1999 Coupled Vegetation and Urban Image (CVUI) of the Moore, Oklahoma Tornado-impacted region.

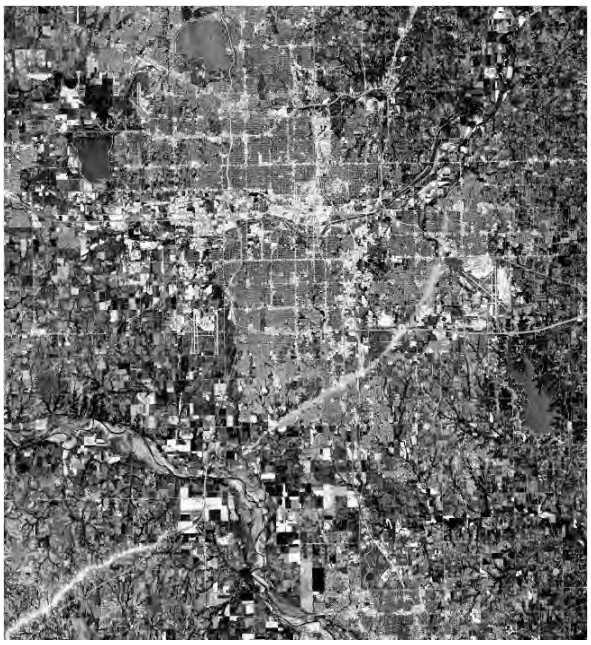

Fig. 7. 1999 Urban Index (UI) of the Moore, Oklahoma Tornado-impacted region.

Fig. 8. 1999 Normalized Difference Vegetative Index (NDVI) of the Moore, Oklahoma Tornado-impacted region.

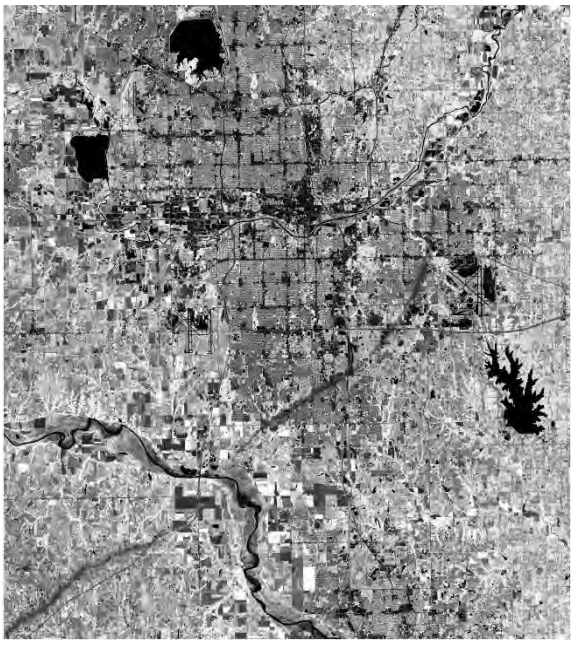

Fig. 9. 1999 Soil Adjusted Vegetative Index (SAVI) for the Moore, Oklahoma Tornado-impacted region.

Fig. 10. 1999 Shortwave Infrared Vegetative Index (SWIRI) for the Moore, Oklahoma Tornado-impacted region.

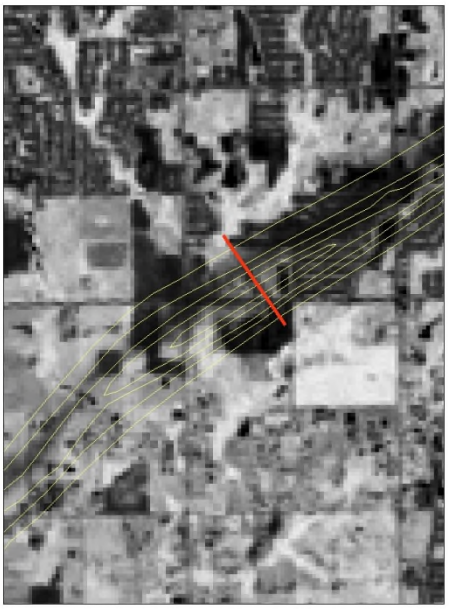

Fig. 11. 1999 Urban Index showing the transect for 1999 Moore, Oklahoma Tornado-impacted region right after the tornado disaster.

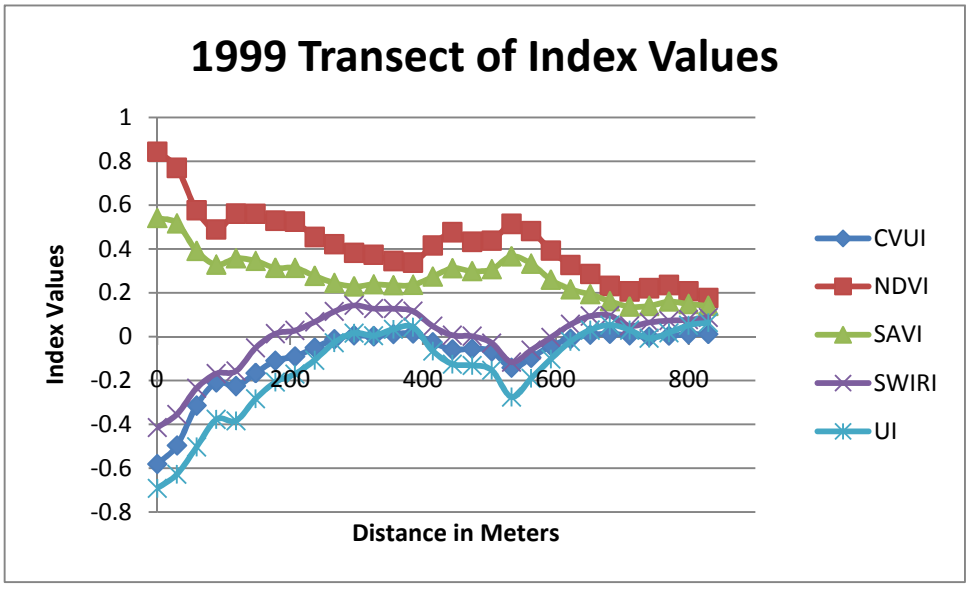

Fig. 12. Transect of Damaged Area affected by the 1999 Moore, Oklahoma 4.3

4.3 Performance of the Recovery Index

Although the post-tornado images displayed virtually identical damage patterns, the recovery images highlighted some significant differences between the indices in terms of the extent of reconstruction. Most notably, both vegetation indices indicate faster reconstruction than the CVUI, SWIRI and UI recovery images as seen in Figures 13 – 27. While NDVI and SAVI continue to show extensive damages similar to CVUI, SWIRI and UI for 2000, the 2001 recovery images show only minor damages in the residential sections located in the upper portion of the track and some of the forested regions in the lower left quadrant. Contrary to the vegetation indices, damage remains more widespread for CVUI, SWRI and UI scenes in 2001 particularly in the upper right and lower left sections of the track (Figs. 13-27). Even more contrast between the 2002 recovery patterns exists with the vegetation indices showing almost complete recovery with only slight damage to the left of the airport and in the densely vegetative areas of the lower left quadrant. Contrary to this pattern, the other indices show only minor recovery changes in 2002 from 2001 with damage still visible in the residential areas to the left of the airport as well as to the southwest (north of the river) and in the vegetative areas in the lower left portion of the image.

Unlike the vegetation indices, there were some subtle differences in reconstruction among the CVUI, SWIRI and UI recovery images. Overall, both SWIRI and UI displayed nearly identical damage patterns with some discernable differences with the CVUI recovery scenes (Figs. 13 - 18, 25 - 27). Both SWIRI and UI showed slightly more damage in some of the residential areas to the north of the river compared to CVUI in 2000. For the following year, more damage can

be seen in the urban areas located in the upper portion of the track with SWIRI and UI images. However, in the CVUI scene, there appears to be slightly more damage than both the SWIRI and UI images in the vegetative areas near the lower left corner.

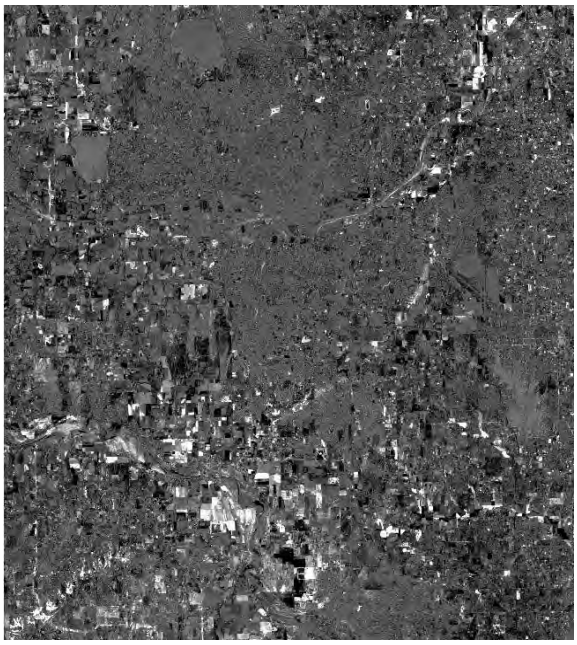

Fig. 13. 2000 Recovery Image of Coupled Vegetation and Urban Image CVUI of the 1999 Moore, Oklahoma Tornado-impacted region.

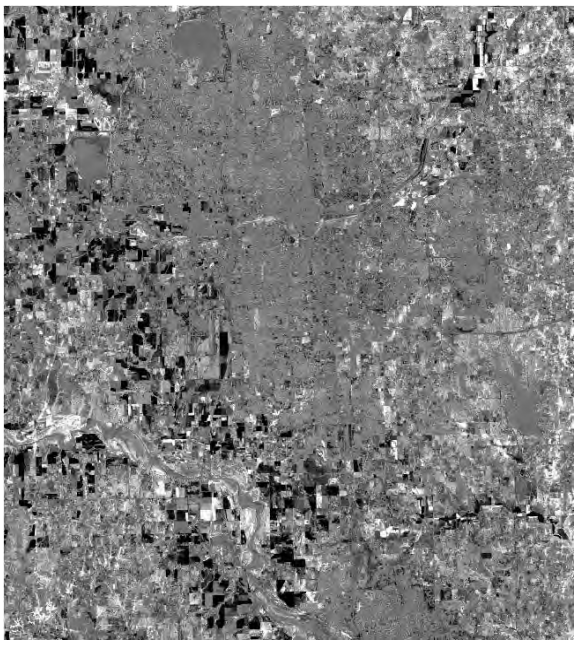

Fig. 14. 2001 Recovery Image of Coupled Vegetation and Urban Image CVUI of the 1999 Moore, Oklahoma Tornado-impacted region.

Fig. 15. 2002 Recovery Image of Coupled Vegetation and Urban Image CVUI of the 1999 Moore, Oklahoma Tornado-impacted region.

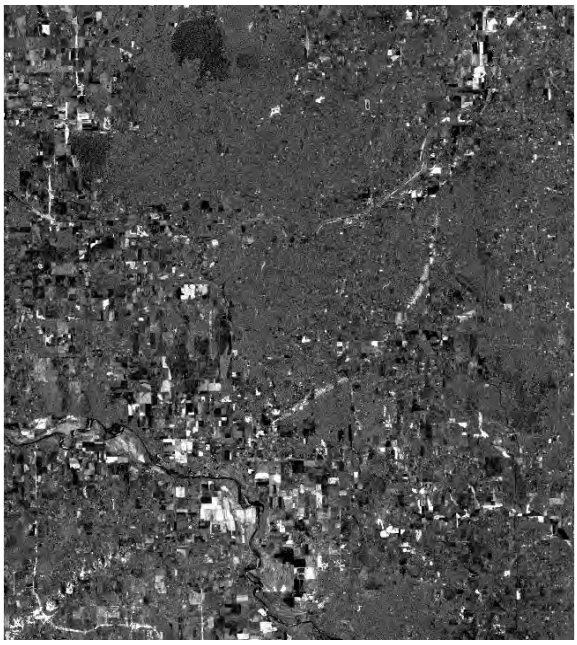

Fig.16. 2000 Recovery Image of the Urban Index (UI) of the 1999 Moore, Oklahoma Tornado-impacted region.

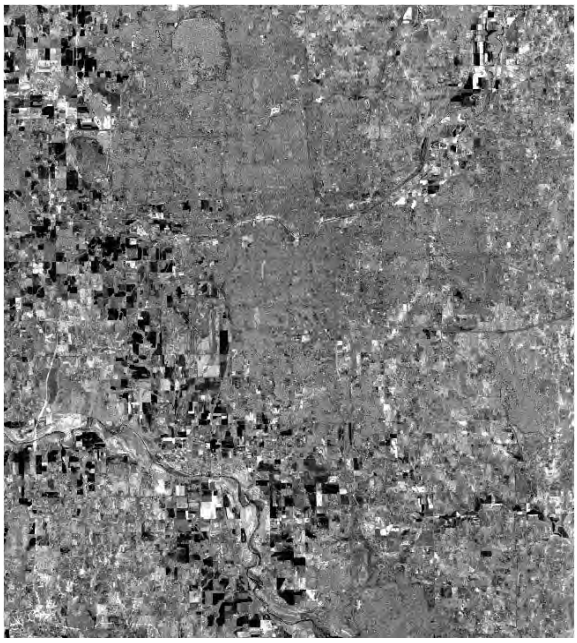

Fig. 17. 2001 Recovery Image of the Urban Index (UI) of the 1999 Moore, Oklahoma Tornado-impacted region.

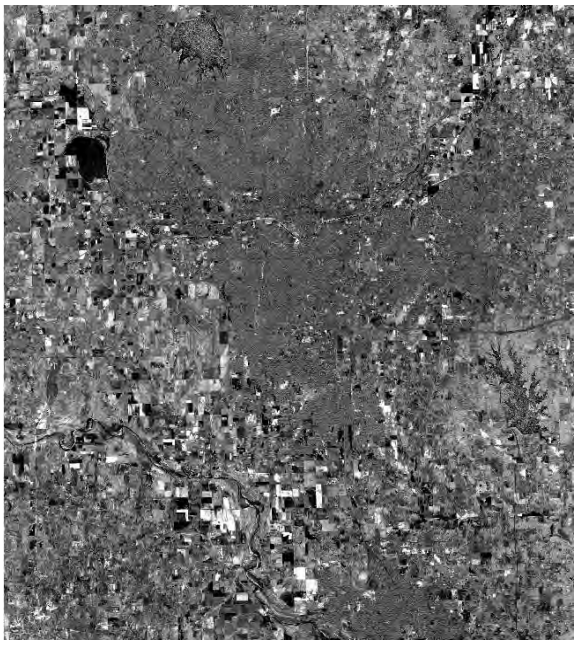

Fig.18. 2002 Recovery Image of the Urban Index (UI) of the 1999 Moore, Oklahoma Tornado-impacted region.

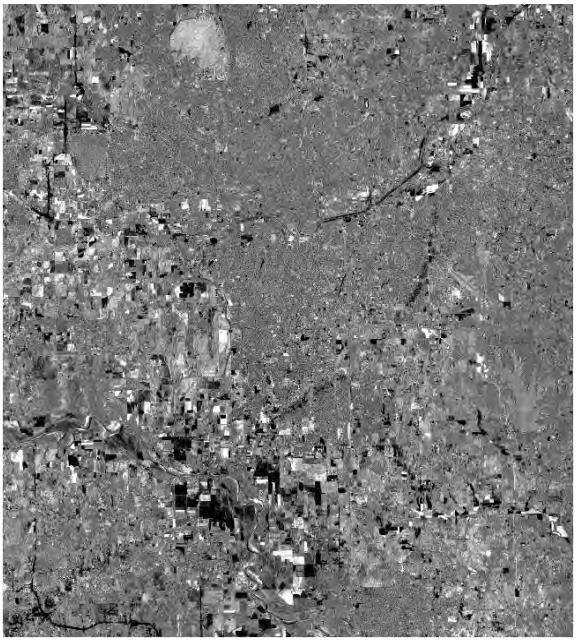

Fig. 19. 2000 Recovery Image of Normalized Difference Vegetative Index (NDVI) of the 1999 Moore, Oklahoma Tornado-region.

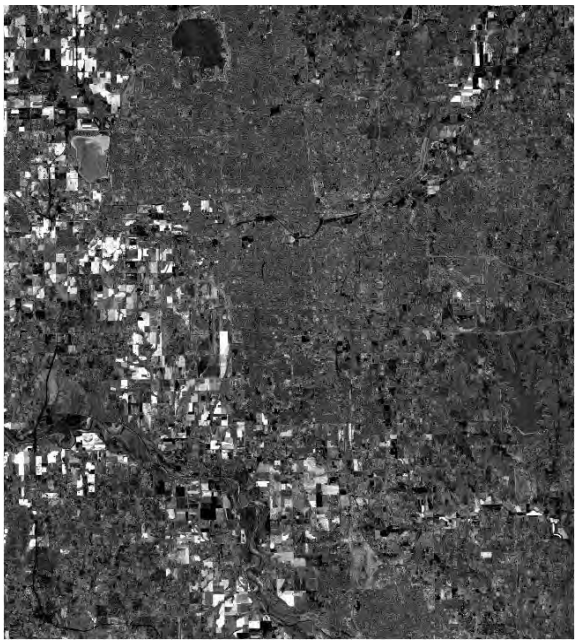

Fig. 20. 2001 Recovery Image of Normalized Difference Vegetative Index (NDVI) of the 1999 Moore, Oklahoma Tornado-impacted region.

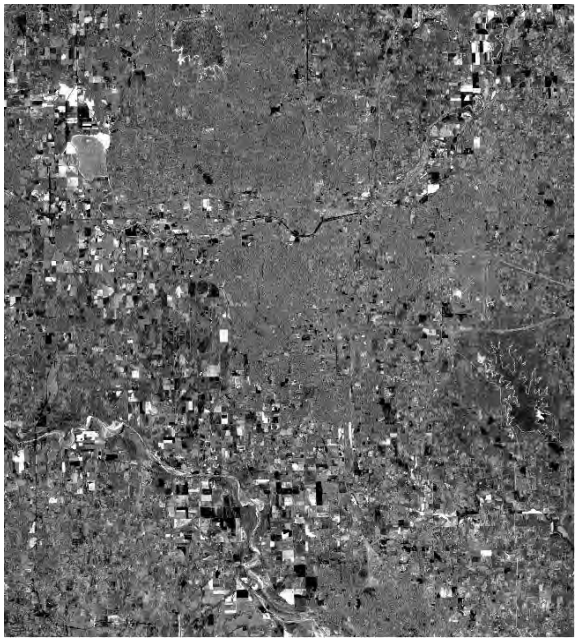

Fig. 21. 2002 Recovery Image of Normalized Difference Vegetative Index (NDVI) of the 1999 Moore, Oklahoma Tornado-impacted region.

Fig. 22. 2000 Recovery image of Soil Adjusted Vegetative Index (SAVI) of the 1999 Moore, Oklahoma Tornado-impacted region.

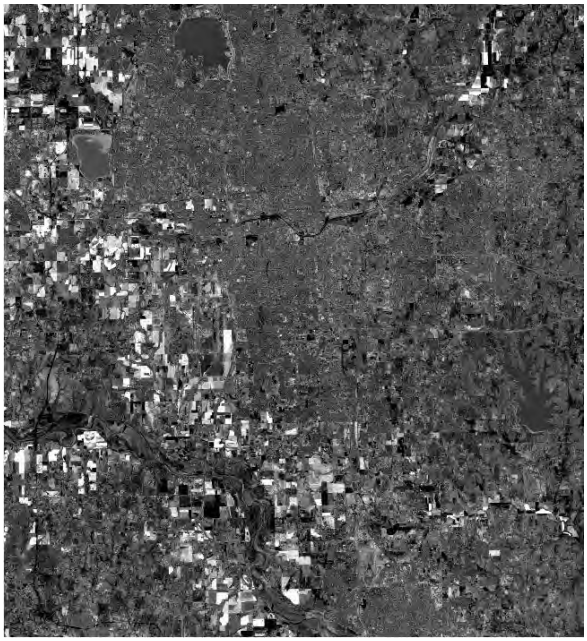

Fig . 23. 2001 Recovery image of Soil Adjusted Vegetative Index (SAVI) of the 1999 Moore, Oklahoma Tornado-impacted region.

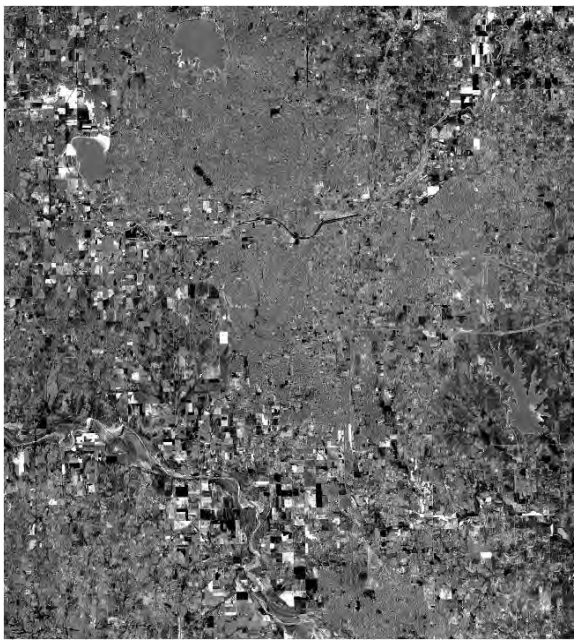

Fig. 24. 2002 Recovery image of Soil Adjusted Vegetative Index (SAVI) of the 1999 Moore, Oklahoma Tornado-impacted region.

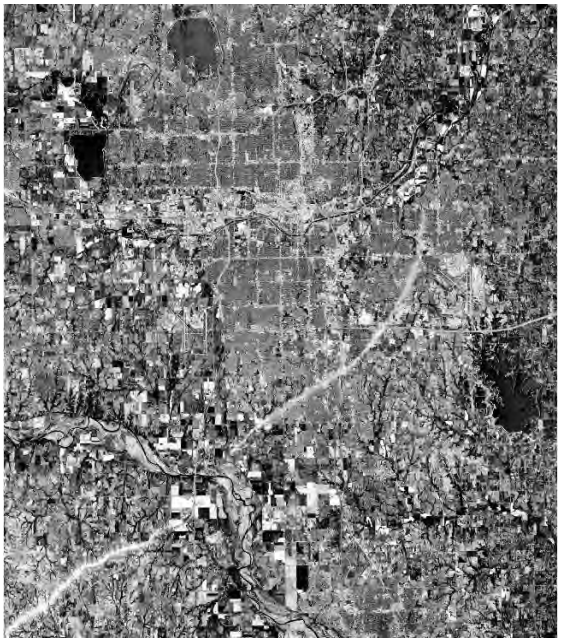

Fig. 25. 2000 Recovery image of the Shortwave Infrared Index (SWIRI) of the 1999 Moore, Oklahoma tornado-impacted region.

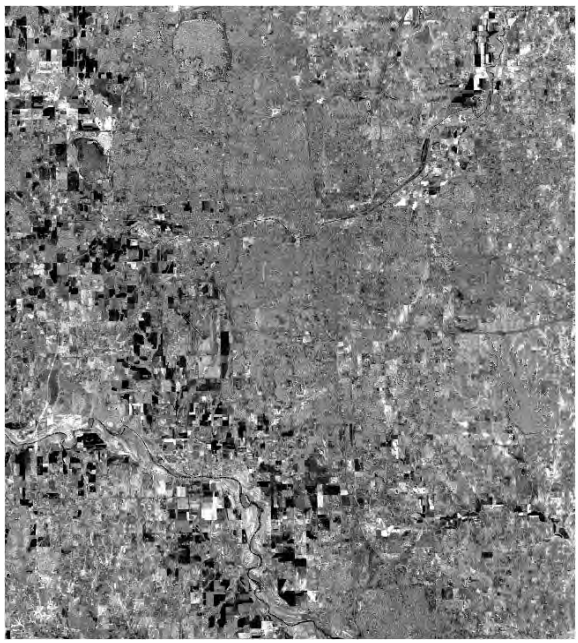

Fig. 26. 2001 Recovery image of the Shortwave Infrared Index (SWIRI) of the 1999 Moore, Oklahoma tornado-impacted region.

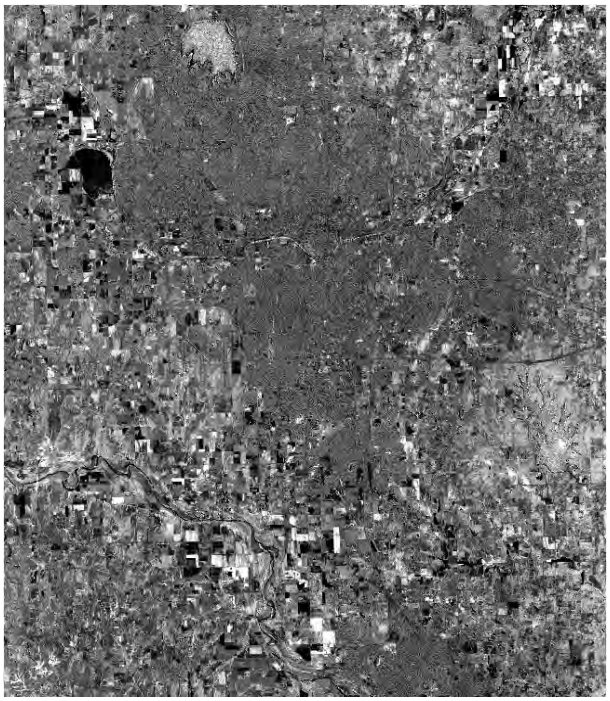

Fig.27. 2002 Recovery image of the Shortwave Infrared Index (SWIRI) of the 1999 Moore, Oklahoma tornado-impacted region.

For 2002, the only minor difference between the CVUI, SWIRI and UI images is a slightly stronger damage pattern in the urban areas in the upper section of the track of both SWIRI and UI scenes.

Accuracy assessments of the aforementioned indices and recovery thresholds revealed several trends. Overall, the 0.5 standard deviation threshold performed poorly among all the indices with an average overall accuracy of 70.13% based on results listed in Table 4. Within this assessment, the vegetation indices were found to be the least effective indices with an average overall accuracy of 66.83% with the lowest overall accuracies of 61.00% and 65.00% with SAVI for 2000 and 2001 respectively. With only a few exceptions, both the 1.0 and 1.5 standard deviation thresholds were more effective at discerning reconstruction by an average of 8.0% with overall accuracies above 80.00% for UI, SWIRI and CVUI. In particular, CVUI and SWIRI yielded the best results with overall accuracies of 86.00%, 85.00% and 84.00% for CVUI at 1.5 for 2000, 1.0 for 2000 and 1.0 for 2002 followed by 84.00% for both SWIRI 1.5 for 2002 and UI 1.5 for 2000. In addition to the trends of thresholds and spectral enhancement types, both 2000 and 2002 recovery images generally reported 3.04% higher overall accuracies on average than the 2001 recovery images.

The same trend remained evident with the average overall accuracy assessments according to the three recovery years by each spectral enhancement type and threshold combination listed in Table 5. Again, the threshold values of 1.0 and 1.5 standard deviations were more effective at discerning recovery compared to the 0.5 standard deviation thresholds (Table 5). The latter threshold

performed poorly among all the indices with the least effective results of 65.00% and 68.67% produced by both SAVI and NDVI. Overall, both vegetation indices underperformed with their best accuracies of 75.67% and 76.33% respectively still short of the 80% land use/ land change classification (Hord 1976).

Table 4. Accuracy Assessments listed by Index, Standard Deviation Threshold and Year. (Overall = Overall accuracy, Producer's. = Producer's accuracy, User's = User's Accuracy)

			Recovery		Damaged		Overall	
Index	StDev	Year	Producer's	User's	Producer's	User's	Overall	Kappa
NDVI	0.5	2000	61.73%	100.00%	100.00%	38.00%	69.00%	0.3800
NDVI	0.5	2001	63.51%	94.00%	88.46%	46.00%	70.00%	0.4000
NDVI	0.5	2002	65.79%	100.00%	100.00%	48.00%	74.00%	0.4800
NDVI	1	2000	66.22%	98.00%	96.15%	50.00%	74.00%	0.4800
NDVI	1	2001	69.57%	96.00%	93.55%	58.00%	77.00%	0.5400
NDVI	1	2002	71.88%	92.00%	88.89%	64.00%	78.00%	0.5600
NDVI	1.5	2000	71.64%	96.00%	93.94%	62.00%	79.00%	0.5800
NDVI	1.5	2001	73.44%	94.00%	91.67%	66.00%	80.00%	0.6000
NDVI	1.5	2002	75.81%	94.00%	92.11%	70.00%	82.00%	0.6400
SAVI	0.5	2000	56.47%	96.00%	86.67%	26.00%	61.00%	0.2200
SAVI	0.5	2001	74.24%	98.00%	97.06%	66.00%	82.00%	0.6400
SAVI	0.5	2002	77.97%	92.00%	90.24%	74.00%	83.00%	0.6600
SAVI	1	2000	78.33%	94.00%	92.50%	74.00%	84.00%	0.6800
SAVI	1	2001	78.69%	96.00%	94.87%	74.00%	85.00%	0.7000
SAVI	1	2002	84.62%	88.00%	87.50%	84.00%	86.00%	0.7200
SAVI	1.5	2000	60.00%	90.00%	80.00%	40.00%	65.00%	0.3000
SAVI	1.5	2001	64.52%	80.00%	73.68%	56.00%	68.00%	0.3600
SAVI	1.5	2002	63.77%	88.00%	80.65%	50.00%	69.00%	0.3900
SWIRI	0.5	2000	63.01%	92.00%	85.19%	46.00%	69.00%	0.3800
SWIRI	0.5	2001	63.89%	92.00%	85.71%	48.00%	70.00%	0.4000
SWIRI	0.5	2002	65.22%	90.00%	83.87%	52.00%	71.00%	0.4200
SWIRI	1	2000	66.18%	90.00%	84.38%	54.00%	72.00%	0.4400
SWIRI	1	2001	68.33%	82.00%	77.50%	62.00%	72.00%	0.4400
SWIRI	1	2002	66.67%	92.00%	87.10%	54.00%	73.00%	0.4600
SWIRI	1.5	2000	68.12%	94.00%	90.32%	56.00%	75.00%	0.5000
SWIRI	1.5	2001	70.77%	92.00%	88.57%	62.00%	77.00%	0.5400
SWIRI	1.5	2002	75.00%	84.00%	81.82%	72.00%	78.00%	0.5600
UI	0.5	2000	70.15%	94.00%	90.91%	60.00%	79.00%	0.5800
UI	0.5	2001	74.58%	88.00%	85.37%	70.00%	79.00%	0.5800
UI	0.5	2002	74.60%	94.00%	91.89%	68.00%	81.00%	0.6200
UI	1	2000	60.81%	90.00%	80.77%	42.00%	66.00%	0.3200
UI	1	2001	62.32%	86.00%	77.42%	48.00%	67.00%	0.3400

Table 4 Con't								
UI	1	2002	69.57%	96.00%	93.55%	58.00%	69.00%	0.3800
UI	1.5	2000	65.71%	92.00%	86.67%	52.00%	72.00%	0.4400
UI	1.5	2001	67.65%	92.00%	87.50%	56.00%	74.00%	0.4800
UI	1.5	2002	67.65%	92.00%	87.50%	56.00%	74.00%	0.4800
CVUI	0.5	2000	62.34%	96.00%	91.30%	42.00%	75.00%	0.5000
CVUI	0.5	2001	69.70%	92.00%	88.24%	60.00%	76.00%	0.5200
CVUI	0.5	2002	70.15%	94.00%	90.91%	60.00%	76.00%	0.5200
CVUI	1	2000	70.77%	92.00%	88.57%	62.00%	77.00%	0.5400
CVUI	1	2001	72.58%	90.00%	86.84%	66.00%	78.00%	0.5600
CVUI	1	2002	74.19%	92.00%	89.47%	68.00%	80.00%	0.6000
CVUI	1.5	2000	77.19%	88.00%	86.05%	74.00%	81.00%	0.6200
CVUI	1.5	2001	78.33%	94.00%	92.50%	74.00%	84.00%	0.6800
CVUI	1.5	2002	76.56%	98.00%	97.22%	70.00%	84.00%	0.6800

Table 5. Averaged Accuracy Assessments listed by Index and Standard Deviation Threshold. (Overall = Overall accuracy, Prod. = Producer's accuracy, User's = User's Accuracy, R = Rank, PR = Producer's Rank, UR= User's Rank)

		Overall		Recovery				Damaged			
Index	St Dev	Ave.	R	Prod.	User's	PR.	UR	Prod.	User's	PR.	UR
SAVI	0.5	65.00%	15	62.01%	94.00%	15	4	86.74%	41.33%	14	15
SAVI	1.0	75.67%	8	67.32%	93.33%	9	8	89.12%	54.00%	7	10
SAVI	1.5	74.33%	9	67.73%	93.33%	8	8	89.05%	55.33%	8	9
NDVI	0.5	68.67%	14	62.59%	93.33%	14	8	88.21%	44.00%	11	14
NDVI	1.0	76.33%	7	69.49%	94.00%	7	4	90.81%	58.67%	2	7
NDVI	1.5	71.00%	12	66.24%	86.00%	12	15	80.00%	56.00%	15	8
UI	0.5	73.00%	11	66.42%	93.33%	11	8	89.63%	52.67%	6	12
UI	1.0	80.00%	5	74.59%	91.33%	3	12	88.91%	68.67%	9	4
UI	1.5	79.00%	6	72.88%	94.00%	6	4	91.44%	64.67%	1	6
SWIRI	0.5	73.67%	10	66.85%	94.00%	10	4	90.25%	53.33%	4	11
SWIRI	1.0	80.33%	3	74.34%	92.67%	5	10	90.63%	68.00%	3	5
SWIRI	1.5	81.67%	1	77.10%	90.00%	2	14	88.19%	73.33%	12	1
CVUI	0.5	70.33%	13	64.08%	92.67%	13	10	86.77%	48.00%	13	13
CVUI	1.0	80.33%	3	74.53%	92.00%	4	11	89.86%	68.67%	5	3
CVUI	1.5	81.67%	1	77.27%	90.67%	1	13	88.74%	72.67%	10	2

UI was consistently better than SAVI and NDVI with the best threshold of one standard deviation accurately classifying 80% of damaged and recovered pixels followed by 79.67% for the 1.5 standard deviation threshold. Performing even better than UI, both new indices, SWIRI and CVUI, were found to be the most effective indices at capturing yearly reconstruction with the same average overall

accuracies of 80.33% and 81.67% for 1.0 and 1.5 standard deviation thresholds respectively.

Additional accuracy assessments were able to correctly identify recovered regions in terms of the user's accuracies, but had some difficulty with the inclusion of damaged pixels in the recovered class as noted by the producer's accuracies. For all the indices, the user's accuracies were above 86.00% suggesting little difficulty in classifying recovered pixels. The smallest threshold of 0.5 standard deviations outperformed the other thresholds with a user's accuracy of 94.00% for SAVI, NDVI, SWIRI and UI, while the 1.5 standard deviation threshold had the greatest difficulty of misclassifying damaged pixels especially in the case of NDVI. Contrary to the user's accuracy assessments, the largest deviations yielded the best results with producer's accuracies of 77.27% for CVUI followed by 77.10% for SWIRI. The worst producer's accuracies resulted with accuracies below 70.00% from both SAVI and NDVI. Overall, the producer's accuracies had more problems excluding recovered pixels from the damaged class with overall lower results than the user's accuracies.

Unlike recovered regions, damaged pixels were more difficult to classify as noted by both lower producer's and user's accuracy assessments. While producer's accuracies remained at 80.00% or above, these accuracies were still lower than those of recovered pixels by 19.00% on average. The most effective results were produced by the UI at 91.44% using 1.5 standard deviation followed by NDVI and SWIRI at 1.0 standard deviation thresholds with 90.81% and 90.63% respectively. Both 0.5 and 1.5 standard deviation thresholds

underperformed with the least effective results of 80.00% reported with NDVI using the 1.5 standard deviation threshold. Unlike the producer's accuracies, the user's accuracies deviated more with the lowest accuracy of 41.33% noted with SAVI at 0.5 standard deviation to the highest accuracy of 73.33% reported by SWIRI at 1.5 standard deviation threshold. Overall, the largest standard deviation thresholds classified damaged pixels the best using UI, SWIRI and CVUI compared to the vegetation indices.

Although the larger thresholds reported higher overall accuracies, these findings were mixed when examining producer's and user's accuracies for both classified damaged and recovered regions. For recovered pixels, the 0.5 standard deviation threshold had the least problem of including damaged pixels in recovered class with the highest user's accuracy of 93.47%, while the 1.5 standard deviation threshold had the least problems misidentifying recovered pixels as damaged with the highest producer's accuracy of 72.24%. For damaged pixels, the 1.0 standard deviation threshold noted the highest producer's accuracy of 89.87%, while 1.5 standard deviation threshold reported the highest user's accuracy of 64.40%. Overall, the narrower ranges had fewer problems misidentifying pixels, while the larger ranges were more susceptible to the inclusion of the wrong class of pixels. However, the larger thresholds could be less affected by exogenous land use changes such as agricultural practices and newly built-environments.

4.4 Annual Reconstruction and Recovery Rates

Based on the top six overall accuracy assessments, maps depicting reconstruction over three years portrayed similar recovery trends. These maps shown in Figures 28 – 33 all suggested complete recovery was never achieved by 2002 with an average of 91.14% recovered in 2002 based on recovery information listed in Tables 6. In fact, the majority of reconstruction occurred within the first two years after the disaster by an average of 79.27% with only an 11.87% increase in 2002. Similar damaged patterns also remained with the vegetative regions still affected in the lower left quadrant and just south of the river and residential sections located to the northeast of the river and to the left of the airport (Figs. 28 - 33).

The type of differences between the recovery maps (Figs. 28 - 33) was mainly impacted by the threshold selection followed by the spectral enhancement type (CVUI, NDVI, SAVI, SWIRI, UI). The 1.5 standard deviation threshold illustrated more reconstruction overall with 94.24% recovered by 2002 compared to only 88.05% recovered using the 1.0 standard deviation threshold. The different thresholds also highlighted deviations in annual recovery rates with the 1.5 standard deviation threshold depicting 12.70% more recovery in 2000 compared to the 1.0 standard deviation threshold. Although the latter threshold portrayed 4.41% more reconstruction in 2001, the former threshold still captured 8.29% more recovery. The former threshold also handled land use changes better particularly in the case of agricultural fields, which can be seen as distinct linear shapes in McClain County. These regions were predominantly classified as

recovered in 2001 using the former threshold, where as the latter threshold consistently classified these regions as still damaged even in 2002.

Table 6. Annual Recovery Rates listed by Index, Threshold (Thres.) and Year.

Index	Thres.	Year	Recovered Area (km)	Damaged Area (km)	Total Area (km)	Recovery Rate (%)
SWIRI	1.5	2000	24,362.10	6,975.90	31,338.00	77.74%
		2001	28,655.10	2,682.90	31,338.00	91.44%
		2002	29,631.60	1,706.40	31,338.00	94.55%
	1.0	2000	20,372.40	10,965.60	31,338.00	65.01%
		2001	25,909.20	5,428.80	31,338.00	82.68%
		2002	26,928.90	4,409.10	31,338.00	85.93%
CVUI	1.5	2000	24,804.90	6,533.10	31,338.00	79.15%
		2001	28,607.40	2,730.60	31,338.00	91.29%
		2002	29,391.30	1,946.70	31,338.00	93.79%
	1	2000	20,815.20	10,522.80	31,338.00	66.42%
		2001	26,239.50	5,098.50	31,338.00	83.73%
		2002	27,894.60	3,443.40	31,338.00	89.01%
UI	1.5	2000	24,124.50	7,213.50	31,338.00	76.98%
		2001	28,357.20	2,980.80	31,338.00	90.49%
		2002	29,575.80	1,762.20	31,338.00	94.38%
	1.0	2000	20,161.80	11,176.20	31,338.00	64.34%
		2001	25,674.30	5,663.70	31,338.00	81.93%
		2002	27,952.20	3,385.80	31,338.00	89.20%

Spectral enhancement types (CVUI, NDVI, SAVI, SWIRI, UI) were also affected by land cover changes with some noticeable differences determining recovery in the vegetative regions and urban areas. Focusing on the 1.5 threshold results, both the CVU and SWIR indices illustrated slightly more damage in the urban areas located in the upper portion of the track as well as less damage in the vegetative regions found in the lower portion of the track (Figs. 29 and 31).

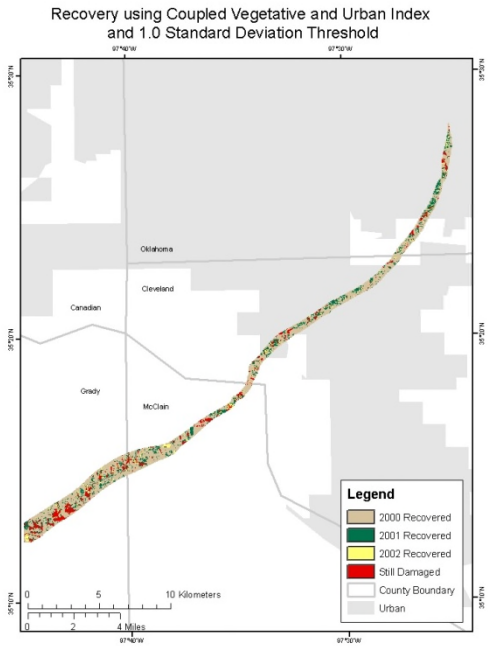

.

Fig. 28. Map of the 1999 Moore Oklahoma Tornado-impacted region showing recovered and damaged regions for 2000, 2001 and 2002 using the Coupled Vegetative and Urban Index (CVUI) and 1.0 standard deviation threshold.

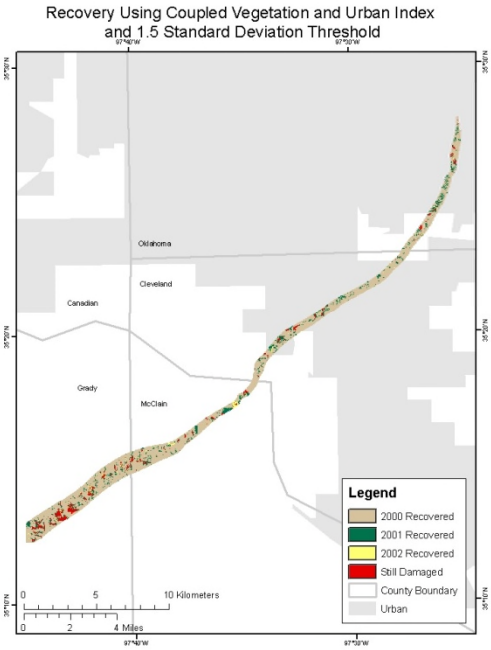

Fig. 29. Map of the 1999 Moore Oklahoma Tornado-impacted region showing recovered and damaged regions for 2000, 2001 and 2002 using the Coupled Vegetative and Urban Index (CVUI) and 1.5 standard deviation threshold.

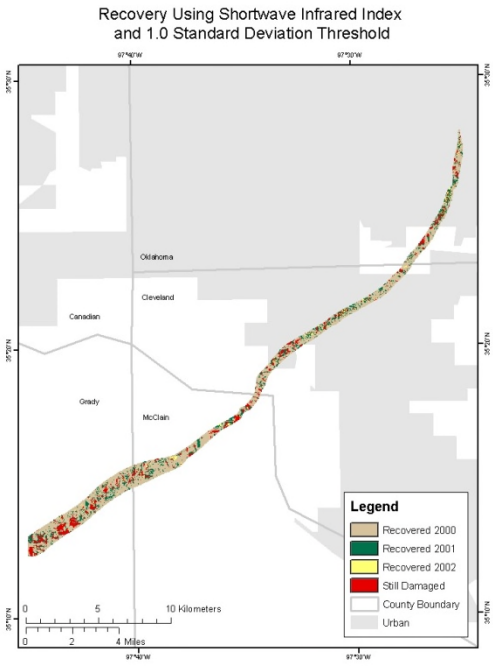

Fig. 30. Map of the 1999 Moore Oklahoma Tornado-impacted region showing recovered and damaged regions for 2000, 2001 and 2002 using the Shortwave Infrared Index (SWIRI) and 1.0 standard deviation threshold.

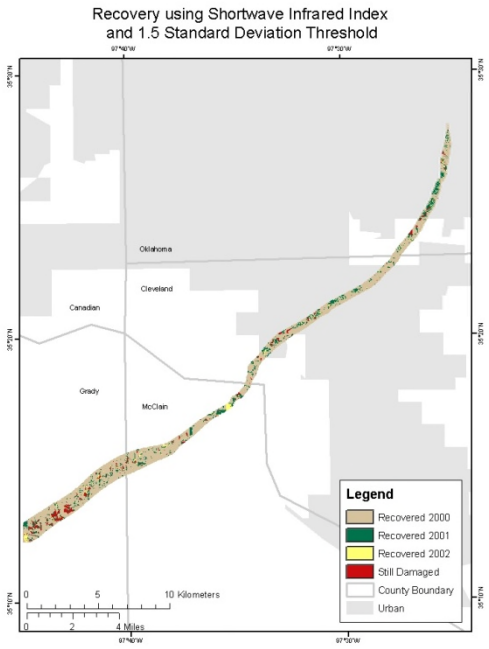

Fig. 31. Map of the 1999 Moore Oklahoma Tornado-impacted region showing recovered and damaged regions for 2000, 2001 and 2002 using the Shortwave Infrared Index (SWIRI) and 1.5 standard deviation threshold.

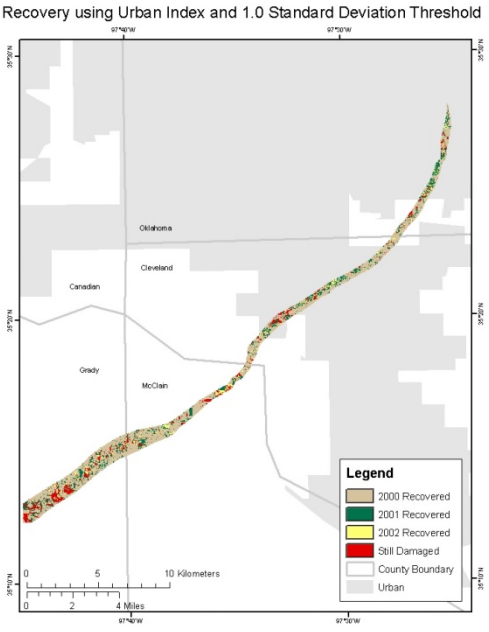

Fig. 32. Map of the 1999 Moore Oklahoma Tornado-impacted region showing recovered and damaged regions for 2000, 2001 and 2002 using the Urban Index (UI) and 1.0 standard deviation threshold.

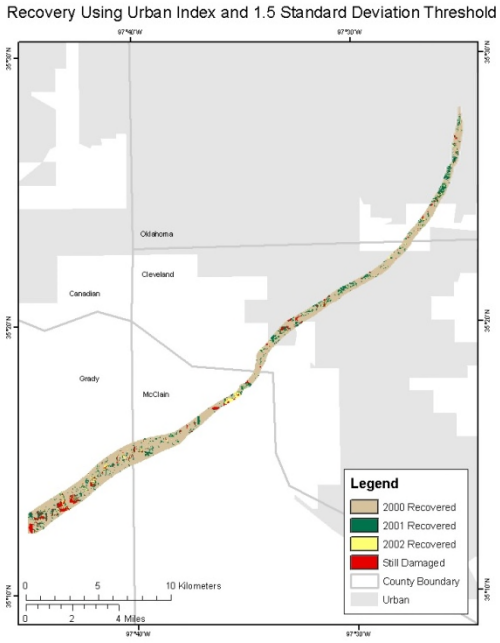

Fig. 33. Map of the 1999 Moore Oklahoma Tornado-impacted region showing recovered and damaged regions for 2000, 2001 and 2002 using the Urban Index (UI) and 1.5 standard deviation threshold.

Although CVUI and SWIRI displayed nearly identical damage patterns, more damage can be seen in urban areas in the top of the track in the case of CVUI (Fig. 29). CVUI, in particular, had the least problem in misclassifying agricultural changes as damaged areas when comparing the bottom portion of the track to the other indices, whereas, UI proved to be the most problematic with more fields misidentified as damaged in the middle and bottom portions of the track. Other differences among the indices could be seen in annual recovery rates

with the CVUI, SWIR and UI reporting the largest reconstruction for 2000, 2001 and 2002 respectively (Figs. 27, 29 and 31).

4.5 Recovery Rates as a Function of the Fujita Scale

By establishing recovery through the investigation of different indices and thresholds in the previous analysis, recovery rates were determined to examine whether or not the level of damage played a key role in reconstruction. The first major finding of this analysis for the top six recovery indices and thresholds is the consistent theme that the incredibly damaged regions associated with an F-5 rating were the slowest to recover, while the F0/F1 regions comprised of minor damages reported the highest recovery rates. Specifically, in the first year following the tornado event (2000), recovery from F0/F1-F3 damage occurred by an average 73.45%, while the most substantial damage of F4-F5 only recovered by an average of 58.69%. Even by the third year after the tornado event (2002), recovery for the F5 zone was only 75.32% while F0/F1 damage had recovered to 94.07%.

Individual differences in recovery rates based on F-scale zones were affected by threshold selection and spectral enhancement type as a result of the previous analysis. The main differences were attributed to threshold selection with the 1.5 standard deviation reporting 12.88%, 8.14% and 6.34% more recovery on average for all the indices than the 1.0 standard deviation for 2000, 2001 and 2002 respectively (Table 6). The most significant differences occurred during the first year after the tornado disaster with these deviations tapering off in 2001 and even more so in 2002. However, the SWIR index with the 1.5 standard

deviation threshold reported anomalously higher values in 2002 that varied from 6.54% to 10.58% with the largest rate increase in the F4 zones. As a result, the SWIR index at the 1.5 standard deviation threshold had the highest recovery rates for 2002 with the exception of UI reporting the highest recovery rate for the F5 zone for both thresholds. Despite this result, the CVU index displayed the highest recovery rates overall for both thresholds followed by the SWIR index with the lowest recovery rates reported by UI.

Using the information from the top six recovery results (Table 6), recovery rates for each F-scale zone were averaged for further analysis according to each year after the event. For any particular year (2000-2002), those values (Table 7) illustrated that recovery in the F5 damage zones consistently lagged behind the F0/F1 zone throughout 2000, 2001, and 2002 by a noticeable difference of 22.21%, 17.13% and 18.76% respectively. The recovery rates for the F4 zones were also distinctly lower than the F0/F1 – F3 recovery rates with these lesser-damaged regions exhibiting very similar behavior in terms of slope and range.

When the averaged values were plotted by year (Fig. 34), a significant difference in recovery rates was evident between 2000 and 2001 as opposed to 2001 to 2002 for all damaged levels. The 2000-2001 rates displayed a 12.59% - 18.15% increase in recovery, while the 2001-2002 recovery rates increased from 2.05% to 5.55%. Other deviations regarding slope could be seen from 2001 to 2002 as the F4 zone reported the highest change in recovery by 5.55%, while the F5 recovery rate nearly plateaued with only a 2.05% increase in 2002 with a total

75.32% recovered. Conversely, F0/F1-F3 recovery rates from 2000 to 2002 produced nearly identical slopes and a relatively narrow range.

Table 7. Recovery Rates for F-scale zones listed by Index, Threshold (Thres.) and Year.

Index	Thres.	Year	F-scale Zone	Recovered Area (km)	Damaged Area (km)	Total Area (km)	Recovery Rate(%)
SWIR	1.5	2000	1	8,149.50	1,701.00	9850.5	82.73%
			2	6,468.30	1,744.20	8,212.50	78.76%
			3	6,130.80	1,881.00	8,011.80	76.52%
			4	3,174.30	1,400.40	4,574.70	69.39%
			5	439.20	249.30	688.50	63.79%
		2001	1	9,293.40	557.10	9850.5	94.34%
			2	7,591.50	621.00	8,212.50	92.44%
			3	7,322.40	689.40	8,011.80	91.40%
			4	3,916.80	657.90	4,574.70	85.62%
			5	531.00	157.50	688.50	77.12%
		2002	1	9,544.50	306.00	9850.5	96.89%
			2	7,842.60	369.90	8,212.50	95.50%
			3	7,596.00	415.80	8,011.80	94.81%
			4	4,110.30	464.40	4,574.70	89.85%
			5	538.20	150.30	688.50	78.17%
CVUI	1.5	2000	1	8,298.90	1,551.60	9,850.50	84.25%
			2	6,583.50	1,629.00	8,212.50	80.16%
			3	6,236.10	1,775.70	8,011.80	77.84%
			4	3,231.90	1,342.80	4,574.70	70.65%
			5	454.50	234.00	688.50	66.01%
		2001	1	9,290.70	559.80	9,850.50	94.32%
			2	7,598.70	613.80	8,212.50	92.53%
			3	7,304.40	707.40	8,011.80	91.17%
			4	3,884.40	690.30	4,574.70	84.91%
			5	529.20	159.30	688.50	76.86%
		2002	1	9,502.20	348.30	9,850.50	96.46%
			2	7,786.80	425.70	8,212.50	94.82%
			3	7,512.30	499.50	8,011.80	93.77%
			4	4,051.80	522.90	4,574.70	88.57%
			5	538.20	150.30	688.50	78.17%
SWIR	1.0	2000	1	6,997.50	2,853.00	9,850.50	71.04%
			2	5,411.70	2,800.80	8,212.50	65.90%
			3	5,060.70	2,951.10	8,011.80	63.17%
			4	2,555.10	2,019.60	4,574.70	55.85%
			5	347.40	341.10	688.50	50.46%
		2001	1	8,494.20	1,356.30	9,850.50	86.23%
			2	6,874.20	1,338.30	8,212.50	83.70%
			3	6,583.50	1,428.30	8,011.80	82.17%
			4	3,471.30	1,103.40	4,574.70	75.88%
			5	486.00	202.50	688.50	70.59%
		2002	1	8,831.70	1,018.80	9,850.50	89.66%
			2	7,126.20	1,086.30	8,212.50	86.77%
			3	6,851.70	1,160.10	8,011.80	85.52%
			4	3,626.10	948.60	4,574.70	79.26%

Table 7 Con't

			5	493.20	195.30	688.50	71.63%
CVUI	1.0	2000	1	7,203.60	2,646.90	9,850.50	73.13%
			2	5,516.10	2,696.40	8,212.50	67.17%
			3	5,129.10	2,882.70	8,011.80	64.02%
			4	2,597.40	1,977.30	4,574.70	56.78%
			5	369.00	319.50	688.50	53.59%
		2001	1	8,631.00	1,219.50	9,850.50	87.62%
			2	7,022.70	1,189.80	8,212.50	85.51%
			3	6,612.30	1,399.50	8,011.80	82.53%
			4	3,484.80	1,089.90	4,574.70	76.18%
			5	488.70	199.80	688.50	70.98%
		2002	1	9,081.00	769.50	9,850.50	92.19%
			2	7,411.50	801.00	8,212.50	90.25%
			3	7,118.10	893.70	8,011.80	88.85%
			4	3,784.50	790.20	4,574.70	82.73%
			5	499.50	189.00	688.50	72.55%
UI	1.5	2000	1	8,220.60	1,629.90	9,850.50	83.45%
			2	6,488.10	1,724.40	8,212.50	79.00%
			3	5,998.50	2,013.30	8,011.80	74.87%
			4	3,031.20	1,543.50	4,574.70	66.26%
			5	386.10	302.40	688.50	56.08%
		2001	1	9,228.60	621.90	9,850.50	93.69%
			2	7,527.60	684.90	8,212.50	91.66%
			3	7,261.20	750.60	8,011.80	90.63%
			4	3,817.80	756.90	4,574.70	83.45%
			5	522.00	166.50	688.50	75.82%
		2002	1	9,543.60	306.90	9,850.50	96.88%
			2	7,827.30	385.20	8,212.50	95.31%
			3	7,568.10	443.70	8,011.80	94.46%
			4	4,095.00	479.70	4,574.70	89.51%
			5	541.80	146.70	688.50	78.69%
UI	1	2000	1	7,115.40	2,735.10	9,850.50	72.23%
			2	5,438.70	2,773.80	8,212.50	66.22%
			3	4,941.00	3,070.80	8,011.80	61.67%
			4	2,366.10	2,208.60	4,574.70	51.72%
			5	300.60	387.90	688.50	43.66%
		2001	1	8,490.60	1,359.90	9,850.50	86.19%
			2	6,830.10	1,382.40	8,212.50	83.17%
			3	6,522.30	1,489.50	8,011.80	81.41%
			4	3,361.50	1,213.20	4,574.70	73.48%
			5	469.80	218.70	688.50	68.24%
		2002	1	9,098.10	752.40	9,850.50	92.36%
			2	7,426.80	785.70	8,212.50	90.43%
			3	7,134.30	877.50	8,011.80	89.05%
			4	3,792.60	782.10	4,574.70	82.90%
			5	500.40	188.10	688.50	72.68%

Table 8. Recovery Rates for F-scale zones listed by Index, Threshold and Year.

F-scale Zone	Percent (%) Recovered in 2000	Percent (%) Recovered in 2001	Percent (%) Recovered in 2002
1	77.81%	90.40%	94.07%
2	72.87%	88.17%	92.18%

Table 8 Con't			
3	69.68%	86.55%	91.08%
4	61.77%	79.92%	85.47%
5	55.60%	73.27%	75.32%

When the averaged recovery values were plotted by F-scale damage (Fig. 35), the most recovery at all levels occurred within the first two years after the event with relatively minor changes between 2001 and 2002. Interestingly, the recovery lines were not parallel across all damage levels, indicating that there were differences in the degree of recovery as a function of F-scale damage. The biggest slope was associated with the 2000 recovery line and the smallest slope was displayed by the 2002 recovery line. In particular, in 2002, the plotted values of recovery between F1, F2, F3 and F4 were similar in terms of creating a nearly horizontal line while the F5 values are still substantially lower.

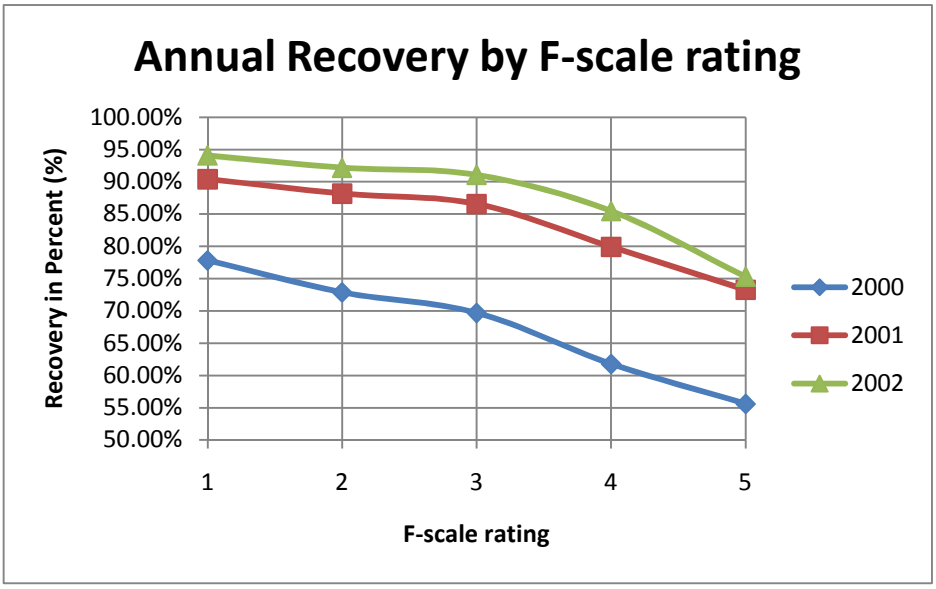

Fig. 34. Graph for the 1999 Moore Oklahoma Tornado-impacted region displaying annual recovery rates for 2000, 2001 and 2002 in percent by F-scale intensity as established by the recovery index.

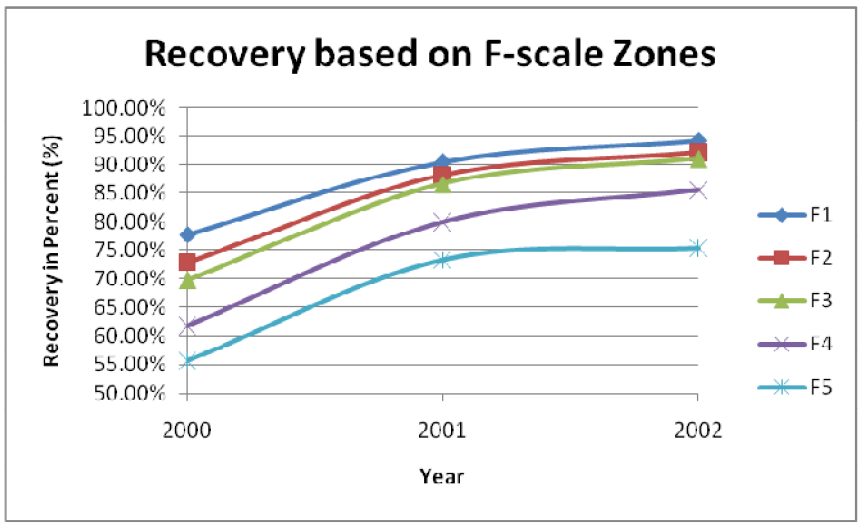

Fig. 35. Graph for the 1999 Moore Oklahoma Tornado-impacted region displaying F-scale recovery rates in percent for 2000, 2001 and 2002 as established by the recovery index.

4.6 Change Vector Analysis

The second change detection method, change vector analysis, investigated the qualitative and quantitative changes for the years of 2000, 2001 and 2002. This approach employed tasseled cap greenness and brightness bands with the possible qualitative changes listed in Table 9. For the first year after the tornado disaster, both class I and IV changes are predominantly seen throughout the track in Figure 36 with relatively small pockets of class II and III types. These changes (Fig. 37) in terms of magnitude were relatively small except for a few isolated spots located in lower left quadrant, middle portion of the track north of the river and upper right portion of the track. Contrary to 2000, the magnitude of change for 2001 (Fig. 38) was considerably higher than the 2000 CVA tasseled cap image as well as more widespread with the largest increases concentrated in the rural areas especially in the vegetative regions in the lower left quadrant and

agricultural areas south of the river. As a result, type IV class changes were observed for every pixel throughout the track, therefore a map was not produced. The 2002 change vector image had very similar changes in terms of magnitude (Figure 39), but observed type II class changes instead of type IV in the entire track.

Table 9. List of land class types and associated land use changes

Class	Type of Change
I	Increase in Greenness, Increase in Brightness
II	Increase in Brightness, Decrease in Greenness
III	Decrease in Greenness, Decrease in Brightness
IV	Decrease in Brightness, Increase in Greenness

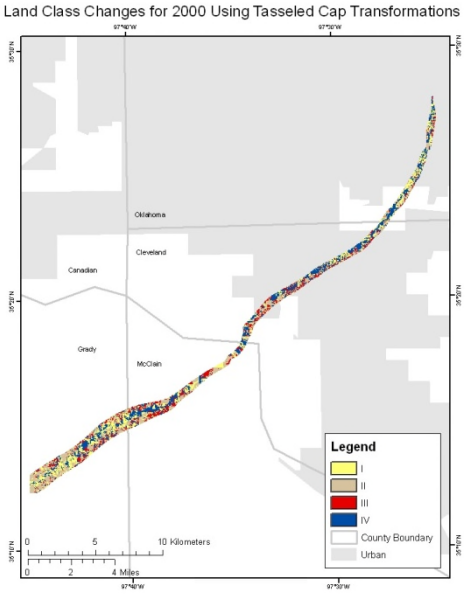

Fig. 36. Change Vector Analysis Map of the 1999 Moore Oklahoma Tornado-impacted region for 2000 showing different land class changes.

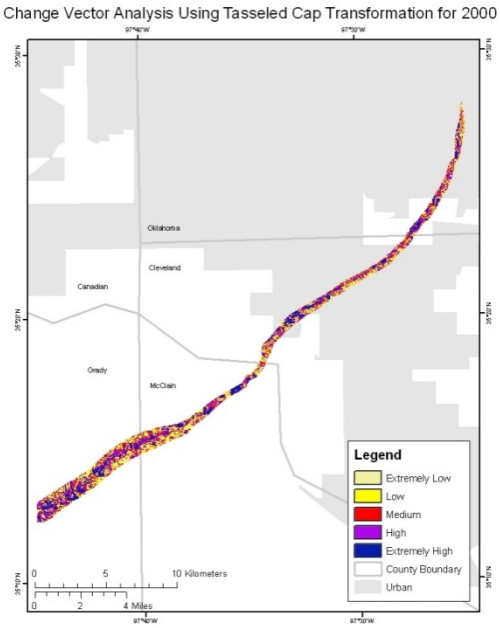

Fig. 37. Map of the 1999 Moore Oklahoma Tornado-impacted region showing the magnitude of changes for 2000 using change vector analysis.

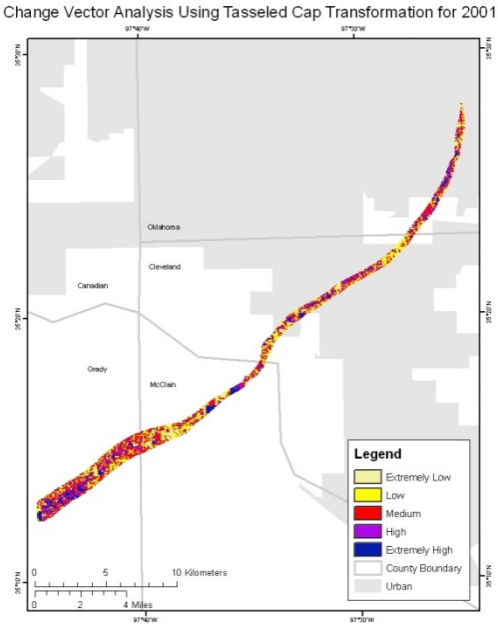

Fig. 38. Map of the 1999 Moore Oklahoma Tornado-impacted region showing the magnitude of changes for 2001 using change vector analysis

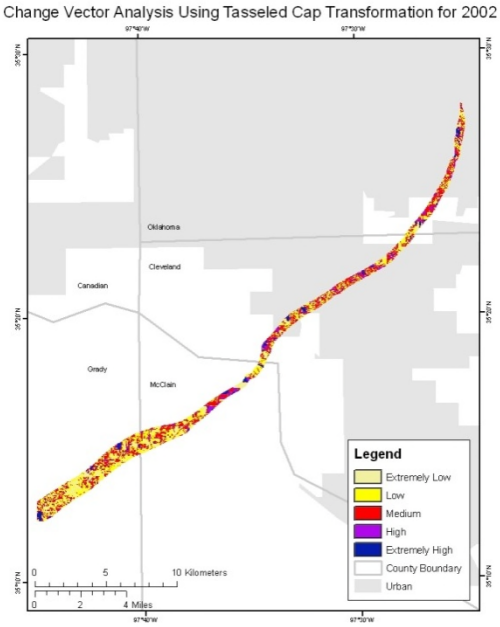

Fig. 39. Map of the 1999 Moore Oklahoma Tornado-impacted region showing the magnitude of changes for 2002 using change vector analysis.

4.7 Conclusion

Reconstruction of the Moore, Oklahoma tornado disaster was examined for the three subsequent years, 2000, 2001 and 2002 following the event using a recovery index by utilizing a series of spectrally enhanced images (NDVI, SAVI, UI, SWIRI, CVUI). This research introduced two new indices, the Coupled Vegetative Index and Urban Index (CVUI) and Shortwave Radiation Index (SWIRI), which proved to be the most effective at assessing reconstruction in conjunction with the 1.5 standard deviation threshold. From these findings, reconstruction maps were created to calculate both annual and Fujita Scale

recovery rates. Annual recovery rates illustrated that complete recovery was never achieved with the majority of reconstruction occurred within the first two years. While these findings held true across all of the F-scale recovery rates, the critical finding in this analysis is that recovery was a direct and significant function of the level of damage sustain, as measured by the Fujita Scale. The most damaged area assessed with an F5 rating consistently lagged in recovery behind the lesser-damaged zones of F0/F1-F3 ratings with the explanation of these findings discussed in the next chapter.

5. Discussion

5.1 Introduction

This research examined the recovery of the Moore, Oklahoma tornado utilizing remote sensing techniques with medium resolution satellite imagery to assess whether or not the level of damage sustained impacted recovery rates as measured by the Fujita Scale. The degree of restoration and recovery was determined by employing a recovery index with different thresholds on a series of transformed images (NDVI, SAVI, UI, SWIRI, CVUI). The findings from this research can be segregated into two broad categories, the results involving the assessment of the recovery index and its effectiveness and the results involving the use of that index in the interpretation of tornado recovery.

With regard to the remote sensing aspect, the first major finding was that medium resolution satellite imagery such as Landsat TM and ETM+ can be used to establish both annual and F-scale recovery rates. Secondly, the two new indices, the Shortwave Infrared Index (SWIRI) and the Coupled Vegetation and Urban Index (CVUI), developed for disaster management and reconstruction proved to be best suited for assessing recovery over the Urban Index (UI), Normalized Difference Vegetation Index (NDVI) and Soil Adjusted Vegetation Index (SAVI). In addition to transformation types, recovery was most effectively captured using the 1.5 standard deviation threshold with the best overall results noted with SWIRI at the same threshold.

With regard to tornado recovery interpretation using these top-performing results, analysis of both annual recovery rates and F-scale recovery rates revealed

two significant findings. The first and most critical finding in this part of my analysis was that the level of damage sustained was a direct and significant function of recovery. The second important finding in this section was that complete recovery was never achieved by 2002 even within the F-scale zones. This chapter discusses the findings of these results.

5.2 Remotely Sensed Data and Recovery Index

Overall, reconstruction of the 1999 Moore, Oklahoma tornado could be discerned using geospatial techniques with medium resolution imagery of Landsat Thematic Mapper and Landsat Enhanced Thematic Mapper (30 meters per pixel). The medium resolution imagery was able to capture the chaotic nature the tornado track effectively by detecting the deviations within regular patterns of spatially arranged ground features such as residential neighborhoods and other urban areas. Using the same premise, reconstruction was then assessed based on changes in the damage pattern on an annual basis for the specific years of 2000, 2001 and 2002. Although detailed damages to individual buildings, roads or trees and reconstruction were not discernable, Landsat imagery considered the recovery of ground features together with the bigger pixel size. Therefore, this imagery provided a top view assessment that could have otherwise been missed with the finer resolution data such as QuickBird or Ikonos imagery.

The degree to which recovery could be accurately discerned proved to be a function of threshold selection and spectral enhancement type. In regards to threshold, average overall accuracy assessments revealed that the 1.0 standard deviation threshold better represented recovery by 78.53% compared to 77.53%

with the 1.5 standard deviation threshold. However, both of these thresholds outperformed the 0.5 standard deviation threshold by an average of 8.00%. This finding suggested that the larger range of values were more reflective of the actual reconstruction similar to previous studies (Roemer et al. 2011, Lin et al. 2004) that also employed thresholds to define damaged and recovered pixels in subsequent recovery year. By employing a threshold with the recovery index, exogenous deviations were minimized due to climate deviations in index values or land use changes, thus reducing the possibility of misclassifying recovered regions as still damaged.

The use of a recovery threshold does pose some limitations in terms of accurately classifying damaged and recovered regions due to range of values representing recovery. Generally, the narrow range of recovered values associated the smaller thresholds had fewer problems misidentifying recovered pixels. However, this threshold had more difficulty accurately classifying damaged pixels. Conversely, the wider range of recovered pixels made the larger thresholds more susceptible to the inclusion of damaged pixels in the recovered class. Despite this limitation, the larger thresholds were more effective at classifying damaged pixels and were able to best capture the recovery process similar to the findings of Roemer et al. 2011 and Lin et al. 2004.

Regardless of threshold selection, damaged pixels proved to be the most difficult to accurately classify due to different land use and land cover changes. In particular, changes in agricultural practices such as fallow versus active field were repeatedly misidentified as damaged when performing classification

accuracy assessments. Additionally, newly constructed urban surfaces were more likely to be misclassified as damaged especially if this transformation occurred in previously healthy vegetation areas. Such a change occurred with the construction of the H.E. Bailey Turnpike Norma Spur (OK 4) in the lower left quadrant of all 2000 recovery images (Figs 13, 16, 19, 22, and 25) and 2000 tasseled cap magnitude image (Figs. 36 and 37). This land use change was repeatedly misidentified as damaged among all the thresholds during the classification accuracy assessments and may have affected the surrounding vegetation creating false damage areas. Consequently, these exogenous changes did affect the overall accuracy of the recovery index, but were rather minimal in comparison to the amount of reconstruction that was accurately identified.

In addition to threshold selection, spectral enhancement type also played a significant role in the performance of the recovery index. The vegetation indices, Normalized Difference Vegetation Index (NDVI) and Soil Adjusted Vegetation Index (SAVI), were the least effective in capturing the recovery process with an average overall accuracy assessment of 66.83%. Although these indices have been extensively employed in disaster studies, damaged and non-damaged areas have been confused in the urban environment due to relatively narrow range of values (Yuan et al. 2002, Jedlovec et al. 2006). Such signature confusion could have hindered correctly identifying recovered pixels during the recovery assessment. Additionally, SAVI and NDVI values can also fall prey to sun illumination effect even with radiometric corrections and normalization. Such differences between years could result in erroneous classification of damaged or

recovered pixels (McDonald et al. 1998, Lu et al. 2004). The composition of vegetation could also affect the ability to discern recovery, as SAVI is generally more suited for densely vegetative areas (Villa 2007). This finding may explain why SAVI consistently reported the lowest accuracies given that prairie grasses and agricultural fields generally dominate this study area with relatively small areas of densely forested regions.

Contrary to the vegetation indices, the Shortwave Infrared Index (SWIRI), the Coupled Vegetation and Urban Index (CVUI) and the Urban Index (UI) were more effective at discerning the recovery process. This finding could be explained, in part, by the use of the mid-infrared bands in conjunction with the near-infrared band with all these indices. The mid-infrared bands (bands 5 and 7) can differentiate between different geology types and urban surfaces, while the near-infrared band measures vegetation health (Lillesand et al. 2004, Sabins 1997, Bentley et al. 2002). As a result, these indices have a wider range of values for non-vegetative surfaces and therefore, could better discriminate between damaged and recovered regions especially in the urban areas. Additionally, the contrast between the tornado track and surrounding areas also made it easier to discern damaged from recovered pixels in the tornado track for each recovery year, thereby improving classification accuracy results.

Among these indices, SWIRI at the 1.5 standard deviation threshold yielded the best results followed by CVUI using the same threshold. Unlike CVUI or UI, SWIRI uses the first mid-infrared band (band 5). This is critical because in addition to discriminating between geology types and urban surface, this band

also measures moisture content in soil and vegetation. Therefore, the use of this band could further discriminate vegetative health as well as discern reconstruction in the built-environment. This may explain why SWIRI outperformed CVUI and UI even though UI and SWIRI had nearly identical damage and reconstruction patterns. Although SWIRI yielded the best results, CVUI better handled vegetative recovery of agricultural fields and densely vegetative areas. This finding could be attributed to a better assessment of vegetation restoration with the NDVI component, as this index is a product of NDVI and UI.

Other factors that could have affected the accuracy of the recovery index were the quality of the images and sampling points for accuracy assessments. For example, cloud-free imagery could not be obtained within the desired two weeks of the anniversary date due to normal springtime storm activity for this region. As a result, atmospheric conditions between images may be different despite radiometric correction attempts to obtain apparent reflectance values for ground features. In addition to atmospheric effects, climate conditions were also significantly different at the acquisition time for 1999, 2000, 2001 and 2002. The first year after the tornado (2000) was an abnormally wet year and then the subsequent years were abnormally dry for April 2001 and September 2002 (OCS 2010b). Although normalization procedures should minimize variations between scenes, some differences could still exist especially in the vegetative areas.

In addition to climate and atmospheric differences, other problems from pixel misregistration and distribution of sampling points could have affected classification accuracies. Locational errors may still exist between scenes despite

co-registration efforts, as complete pixel misregistration is unattainable. While the same approach of stratified random sampling was used, these points were randomly generated and not reused for each accuracy assessment. The location of these points could have a big impact on the accuracy assessment especially if there was a rather high concentration of points in erroneous classified damaged areas such as agricultural fields or on the newly constructed H.E. Bailey Turnpike Norman Spur.

Despite some of these problems, the recovery index was able to correctly identify reconstruction with SWIRI and CVUI using the 1.5 and 1.0 standard deviation thresholds with overall accuracies of 81.67% and 80.33% respectively. The next best results were reported with UI using the larger thresholds with overall accuracies of 80% and 79.33%. Among the best indices, damage patterns were fairly consistent in showing damage in the densely vegetative areas in the lower quadrant and in the urban areas just south of the river and upper portion of track. These regions were some of the hardest hit areas sustaining F4 and F5 damages and would reasonably take longer to recover.

5.3 Recovery Rates as a Function of F-scale

From these top-performing results, I analyzed recovery rates for three years following the 1999 Moore, Oklahoma tornado and established two significant findings. The first and most critical finding in this analysis revealed that the incredibly damaged areas associated with an F-5 rating were the slowest to rebuild, while the lesser-damaged areas of F0/F1 ratings reported the highest recovery rates. These results were consistent throughout 2000, 2001 and 2002 as

reconstruction in F5 damaged areas lagged behind F0/F1 damaged zones by a considerable difference of 22.21%, 17.13%, and 18.76% respectively. The recovery rates for F4 damaged areas were also significantly lower than the F0/F1 – F3 recovery rates for all the recovery years illustrating that the scope and magnitude of the disaster has a profound and direct effect on recovery. This finding is conclusive with other hazard studies (Dacy and Kuerether 1969, Haas et al. 1977, Yasui 2007, Aldridge 2011) that have also found recovery rates to be a function of the biophysical impact.

Higher reconstruction in the F0/F1-F3 damaged areas could be explained by the contrasting differences in associated damages between these regions and those associated with F4 and F5 ratings. Maximum damage indicators for F0/F1-F3 ratings are noted by missing roofs and in some cases removal of walls, while in F-4 rated damaged zones, well-constructed houses are leveled and weaker structures are carried away for some distance (Fujita 1971). Damages associated with F5 ratings are the most severe, as well-constructed structures are leveled and carried away, trees debarked and automobile-sized missiles are generated (Fujita 1971). As a result, reconstruction within the lesser-damaged areas (F0/F1 – F3) would typically require less financial resources to draw upon and time in completing the repairs (Dacy and Kunreuther 1969, Yasui 2007, Finch et al. 2010, Aldridge 2011). This would explain the similar reconstruction rates and faster recovery in the F0/F1 – F3 damaged zones. Unlike the lesser-damaged areas, reconstruction in the most severely damaged areas (F4 and F5) would likely require more financial resources and time rebuild. Severely damaged buildings

and other infrastructure would also likely involve decision-making policies regarding construction type, permits and even possibly relocation, therefore requiring more time to complete (Finch et al. 2010).

In addition to anthropogenic reconstruction, vegetation regeneration is a function of the magnitude of damage and plant size. Generally minor-wind damages to vegetation will re-orient or blow over the plant, resulting in only minor disruptions in photosynthetic activity (Bentley et al. 2002). Therefore, much of the vegetation survives and recovers quickly back to the pre-tornado state. Contrary to this, intense winds are more likely to snap the vegetation and consequently destroy it recovering much slower. Additionally, the speed to which vegetation regenerates also depends on plant size before the disaster, as smaller plants such as short grasses or small shrubs tend to recover quicker than large trees (Peterson 2000). Typically, larger vegetation will take several years if not decades for complete restoration based on tree size (Peterson 2000). This aspect explains not only the vegetative response in terms of recovery rates, but also the location of still damaged areas in the bottom portion of the track due to the densely forested region.

Annual recovery, utilizing the F-scale assessment of tornado damages, also revealed that most reconstruction occurred within the first two years. During the first year, the average recovery rate for all F-scale damage zones was 67.55% indicating rather rapid reconstruction over the assessed time period. Typically, after such a disaster, high priority is placed on reestablishing infrastructure and rebuilding structures with minor damages in attempt to return to pre-disaster

conditions (Uitto 1998, Mitchell 1999). Other structures may take longer to rebuild due to available financial resources, amount of disaster relief, and decision-making policies (Finch et al. 2010). This would explain the additional 12.59% - 18.15% increase in recovery from 2000 to 2001. However, for 2001 – 2002, reconstruction only improved by 2.05% to 5.55% indicating that most recovery occurred within the first two years. Recovery probably tapered off due to the timing of insurance settlements and disaster relief payments within the first couple of years, as most rebuilding occurs soon after the distribution of funds. Additionally, temporary housing could also turn into permanent residence as society becomes more settled with time, therefore foregoing complete reconstruction in certain areas.

Within this recovery assessment, the second important finding was that even by 2002, three years after the tornado event, complete recovery was never achieved within any of the F-scale damaged zones. By 2002, the least damaged regions (F0/F1) had rebuilt to 94.07%, while reconstruction in the most incredibly damaged areas (F5) had reached only 75.32%. Part of this reason could be accredited with too short assessment period, given that a subsequent F4 tornado hit the same study area on May 8, 2003, thereby missing any continued reconstruction. Different land use and land changes also could occur during the recovery process as a result of decision-making policies and political institutions seeking to either mitigate future events or help improve current economic status. Additionally, individual decisions to relocate could also impact reconstruction based on damage severity, financial resources, and psychological decisions to

rebuild in the same area. With regards to vegetation regeneration, large-scale vegetation in terms of trees and large shrubs will take several years if not decades to return to pre-tornado conditions, thus contributing to incomplete recovery.

In addition to the biophysical aspect of disaster, pre-existing conditions could also affect recovery in terms of social vulnerabilities and place-based vulnerabilities. Social vulnerabilities consider the pre-existing social conditions of age, race, ethnicity, dwelling type, socioeconomic status, political institutions and other social variables in conjunction with the biophysical impact of the disaster (Liverman 1990, Blaikie et al 1994, Cutter 1996, Cutter 2000, Cutter et al. 2003). Lower socioeconomic status, lack of resources and poor housing quality can magnify the impact of the disaster and consequently affect the ability to fully recover (Liverman 1990, Blaikie et al 1994, Cutter 1996, Cutter et al. 2003). Such examples of this can be seen in the more recent cases of 2004 Tsunami, Hurricane Katrina, the Haitian Earthquake (Kaplan et. al 2009, Cutter et al. 2006). These factors could have contributed to the incomplete reconstruction after the tornado disaster, but were not analyzed in this analysis. Future research would need to examine these social vulnerabilities in conjunction with the biophysical impact for a complete recovery assessment.

Certain geographic locations may also be physically and socially susceptible to a given hazard creating place-based vulnerabilities (Liverman 1990, Cutter 1996). These regions can have higher degrees of vulnerability based on the clustering of social and biophysical characteristics within the hazard zone (Cutter et al. 2000). The city of Moore, Oklahoma was previously struck by a tornado in

October 1998, but that tornado produced considerably smaller damages with a maximum F-scale rating of F2 and path length of only 2 miles. Nonetheless, this could have affected individual and commercial decisions with regard to rebuilding or re-locating. One known example occurred in a residential section of Moore, Oklahoma as decision-makers chose not to rebuild in this section due to the past occurrence of tornadoes in this area and instead dedicated the land as a city park. Other place-based vulnerabilities, similar to the aforementioned, could have also existed within the track and affected individual and policy-making decisions on reconstruction given the short time between disasters.

5.4 Conclusion

This research examined the reconstruction of the 1999 Moore, Oklahoma tornado for the years of 2000, 2001, and 2002 utilizing remote sensing imagery and change detection methods. The use of medium resolution imagery provided to top-view assessment of reconstruction in which recovery was determined employing a recovery index and different thresholds on a series of spectrally enhanced images (NDVI, SAVI, UI, SWIRI, CVUI). With these spectrally enhanced images, the two new indices, the Shortwave Infrared Index (SWIRI) and the Coupled Vegetation and Urban Index (CVUI), developed for disaster management and reconstruction proved to be best suited for assessing recovery over the Urban Index (UI), Normalized Difference Vegetation Index (NDVI) and Soil Adjusted Vegetation Index (SAVI). In addition to transformation types, recovery was most effectively captured using the 1.5 standard deviation threshold with the best overall results noted with SWIRI at the same threshold. This

threshold accounted for annual deviations between scenes in terms of climate and atmospheric condition and non-damaged land use changes mainly in agricultural areas.

From these top-performing results, I analyzed the recovery rates and established two significant findings. The most critical finding in this research discovered that most severely damaged areas associated with an F5 rating were the slowest to recover, while the lesser damaged areas associated with F0/F1 ratings were the quickest to recover. These results were consistent throughout 2000, 2001 and 2002 as reconstruction for F5 zones consistently lagged the F0/F1 zones by 22.15%, 17.13%, and 18.76% respectively. Recovery rates for F4 damaged areas were also significantly lower than those of the lesser damaged areas (F1-F3) for all the recovery years illustrating that the scope and magnitude of the disaster has a profound and direct effect on recovery. Within these findings, the second important finding was that even by 2002, three years after the disaster, complete recovery was never attained within any of the F-scale damaged zones. The next chapter briefly summarizes this entire project and provides suggestions for future work.

6. Summary and Conclusion

6.1 Summary

This research examined the reconstruction of the 1999 Moore, Oklahoma tornado for the specific years of 2000, 2001, and 2002 from two aspects. The first aspect sought to investigate the recovery process from a remote sensing approach to see if reconstruction could be discerned using geospatial techniques in conjunction with medium resolution imagery. These techniques used different spectral enhancements (NDVI, SAVI, UI, SWIRI, CVUI) and employed a recovery index and different thresholds to assess the recovery process. From these top-performing results, the second aspect took a hazard approach and explored whether or not recovery rates, as measured by the Fujita Scale, were dependent on the scope and magnitude of the biophysical impact. My hypotheses were that medium resolution imagery could effectively detect the recovery process by providing a top-view assessment and that recovery rates were a significant and direct function of the tornado disaster according to the level of damage sustained. The results of this two-part analysis were able to successfully validate both of my hypotheses with the key findings listed below

With regards to the remote sensing component, the first major finding was that medium resolution such as Landsat TM and ETM+ was able to effectively capture the recovery process and can be used to establish both annual and F-scale damage recovery rates. Secondly, the two new indices, Shortwave Infrared Index (SWIRI) and the Coupled Vegetation and Urban Index (CVUI) that I developed for disaster assessment and recovery analysis proved to be the most effective at

discerning reconstruction over the Normalized Difference Vegetation Index (NDVI), Soil Adjusted Vegetation Index (SAVI) and the Urban Index (UI). This analysis also found that the 1.0 and 1.5 standard deviation thresholds were most effective at capturing recovery with the best results depicted by SWIRI using the 1.5 standard deviation threshold.

Using these top-performing results, tornado recovery interpretation yielded two significant findings. The first and most critical finding in this research was that the degree of damage proved to be a direct and significant function of recovery. The most incredibly damaged areas associated with an F5rating were the slowest to rebuild, while the lesser damaged areas associated with an F0/F1 rating were the quickest to recover. This finding was consistent for the assessed recovery years of 2000, 2001 and 2002 as recovery in the F5 damaged zones lagged behind the F0/F1 damaged areas by 22.15%, 17.13%, and 18.76% respectively. This relationship was also evident with the severely damaged areas of an F4 rating as reconstruction was significantly lower than the lesser-damaged regions (F0/F1-F3) for all recovery years illustrating the impact that disaster has in terms of the scale and magnitude on recovery. The second important discovery was that even by 2002, complete reconstruction was never achieved even with the lesser-damaged areas of (F0/F1-F3).

6.2 Suggestions for Future Research

Future research should compare this top-view assessment approach with finer resolution data or other detailed data such as county approved building permits to validate these findings. Other analyses could expand upon this

research by including socioeconomic data such as census block data and parcel information from county assessors' offices to provide a complete assessment of both the physical and social components to the recovery process. In addition to social vulnerabilities, place-based vulnerabilities could also be analyzed to examine regional differences in recovery in conjunction with the biophysical impact. With these future research endeavors, the period of recovery assessment could be extended in order to capture the complete recovery analysis provided the availability of quality data can be acquired.

6.3 Significance

These findings illustrate the need to examine not just the impact of small-scale disasters such as a tornado, but also stress the importance that the scope and magnitude of the disaster has on the recovery process. Decision makers and other policyholders could better understand the importance of the biophysical impact and implement more resilient approaches to reconstruction within the most severely damaged areas.

With regards to remote sensing capabilities, this research sets forth the direction of recovery analysis for tornado disasters using cost effective resolution imagery such as Landsat TM and ETM+ in conjunction with geospatial techniques. This type of analysis provides a top-view assessment that could aid decision-making processes in urban planning and developers in the reconstruction process. Within this research, the two indices, SWIRI and CVUI, developed for disaster management and reconstruction analysis should also be explored with the

traditionally employed indices (NDVI, SAVI, UI) to better capture both the initial impact and recovery process.

REFERENCES

Adger, W. N., 1997: Sustainability and social resilience in coastal resource use. *Global Environmental Change Working Paper 97-23*. Centre for Social and Economic Research on the Global Environment, University of East Anglia and University College London.

Adger, W.N., 2006: Vulnerability. *Global Environmental Change* 16 (3), 268-281.

Aldride, D. P., 2011: The power of people: social capital's role in recovery from the Kobe Earthquake. *Natural Hazards* 56, 595-611.

Alexander, D., 1991: Natural Disasters: A Framework for Research and Teaching. *Disasters* 15(3), 209-226.

Alexander, D. E., 2000: *Confronting Catastrophe: New Perspectives on Natural Disasters.* New York: Terra.

Barrows, H. H., 1923: Geography as Human Ecology. *Annals of the Association of American Geographers* 13, 1-14.

Belward A. S, Stibig H. J, Eva, H., Rembold, F., Bucha, T., Hartley, A., Beuchle, R., Al-Khudhairy, D., Michielon, M.,and D. Mollicone, 2007: Mapping severe damage to land cover following the 2004 Indian Ocean tsunami using Moderate Spatial Resolution Satellite Imagery. *International journal of Remote Sensing* 28(13–14), 2977–2994.

Bentley, M. L., Mote, T. L. and P. Thebepanya, 2002: Using Landsat to Identify Thunderstorm Damage in Agricultural Regions. *Bulletin of American Meteorological Society* 83, 363 - 376.

Berkes, F., Bankes, N., Marschke, M., Armitage, D., and D. Clark, 2005: Cross-scale institutions and building resilience in the Canadian North. In: Berkes, F., Huebert, R., Fast, H., Manseau, M., and A. Diduck, Editors, *Breaking Ice: Renewable Resource and Ocean Management in the Canadian North*, University of Calgary Press, Calgary, 225-247.

Blaikie, P. and H. C. Brookfield, 1987: *Land Degradation and Society*. London: Routledge.

Blaikie, P., Cannon, T., Davis, I., and B. Wisner, 1994: *At Risk: Natural Hazards, People's Vulnerability, and Disasters*. London: Routledge.

Bluestein, H., 2006: *Tornado Alley*. Oxford University Press, 7 pp.

Boruff, B., Easoz, J., Jones, S., Landry, H., Mitchem, J., and S. Cutter, 2003: Tornado Hazards in the United States. *Climate Research* 24, 103-117.
Brookfield, H.C., 1964: Questions on the Human Frontiers of Geography. *Economic Geography* 40, 283-303.

Brooks, H. E. and C. A. Doswell III, 2000: Normalized damage from major tornadoes in the United States: 1890 – 1999. *Weather and Forecasting* 16(1), 168-175.

Brooks, H. E. and C. A. Doswell III, 2002: Deaths in the 3 May 1999 tornado from a historical perspective. *Weather and Forecasting* 17(3), 354-361.

Brooks, H. E., 2003: On the relationship of tornado path length and width to intensity. *Weather and Forecasting* 17, 611-618.

Brooks, N., 2003: *Vulnerability, Risk and Adaptation: A Conceptual Framework,* Working Paper 38, Tyndall Centre for Climate Change Research, Norwich, UK.

Brookfield, H. C. 1964: Questions on the human frontiers of geography. *Economic Geography* 40, 47-67.

Bruneau, M., Chang, S.E., Eguchi, R.T., Lee, G.C., O'Rourke, T.D., Reinhorn, A.M., Shinozuka, M., Tierney, K.T., Wallace, W.A., and D. Von Winterfeldt, 2003: A framework to quantitatively assess and enhance the seismic resilience of communities, *Earthquake Spectra* 19 (4), pp. 733–752.

Burton, I., Kates, R. W., and G. F. White, 1978: *The Environment as Hazard*. Oxford University Press, New York.

Burton, I., Kates, R. W., and G. F. White, 1993: *The Environment as Hazard (2nd edition)*.Oxford University Press, New York.

Buckle, P., Mars, G., and S. Smale, 2000: New approaches to assessing vulnerability and resiliency. *Australian Journal of Emergency Management* 15(2), 8-14.

Burby, R. J., 2004: Reconstruction/Disaster Planning: United States. *International Encyclopedia of the Social and Behavioral Sciences*, 12841-12844.

Carter, W. N., 1991: *Disaster Management: A Disaster Manager's Handbook.* Manila: Asian Development Bank.

Changnon, S. A., Pielke Jr., R. A., Changnon, D., Sylves, R. T., and Pulwarty, R.,

2000: Human factors explain the increased losses from weather and climate Extremes. *Bulletin of American Meteorological Society* 81, 437–442.

Chavez, P. S., 1988: An improved dark-object subtraction technique for atmospheric scattering correction of multispectral data. *Remote Sensing of Environment* 24, 459–479.

Chou, W. C., Lin, W. T. and C. Liu, 2009: Vegetation recovery patterns assessment at landslides caused by catastrophic earthquake: a case study in central Taiwan. *Environmental Monitoring Assessment* 152, 245–257.

Congalton, R. G., 1991: A Review of Assessing the Accuracy of Classifications of Remotely Sensed data. *Remote Sensing of Environment* 37, 35-46.

Congalton, R. G. and K. Green, 1999, *Assessing the Accuracy of Remotely Sensed Data: Principles and Practices*. Boca Raton, FL: Lewis Publishers: 137 p.

Crist, E. P., and R. C. Cicone, 1984: A physically-based transformation of ThematicMapper data-the TM Tasseled Cap. *IEEE Transactions on Geosciences and Remote Sensing* 22, 256–263.

Crist, E. P., 1985: A TM tasseled cap equivalent transformation for reflectance factor data. *Remote Sensing of Environment* 17, 301-306.

Cross, J., 2001: Megacities and small towns: different perspectives on hazard vulnerability. *Environmental Hazards* 3(2), 63-80.

Cutter, S. L., 1996: Vulnerability to environmental hazards. *Progress in Human Geography* 20(4), 529-539.

Cutter, S. L., 2000: American Hazardscapes: *The Regionalization of Hazards and Disasters*. Washington, D.C.: Joseph Henry Press.

Cutter, S. L., 2003: GI Science, Disasters, and Emergency Management. *Transactions in GIS* 7(4), 439-445.

Cutter, S., Boruff, B., and W.L. Shirley. 2003: Social Vulnerability to environmental hazards. *Social Science Quarterly* 84(2), 242-261.

Cutter, S.L., Emrich, C.T., Mitchell, J.T., Boruff, B., Gall, M., Schmidtlein, M., Burton, C., and G. Melton, 2006: The Long Road Home: Race, Class, and Recovery from Hurricane Katrina. *Environment: Science and Policy for Sustainable Development* 48(2), 8-20.

Cutter, S.L. and Finch, C., 2008: Temporal and spatial changes in social

vulnerability to natural hazards. *Proceedings of the National Academy of Sciences* 105(7*)*, 2301-2306.

Dacy, D., and H. Kunreuther, 1969: *The economics of natural disasters: implication for federal policy.* The Free Press, New York.

Davis, I., 2003: *The Effectiveness of Current Tools for the Identification and Synthesis of Vulnerability and Disaster Risk.* Inter-American Development Bank and Universidad Nacional de Colombia- Sede Manizales Instituto de Estudios Ambientales (IDEA): Manizales (http://idea.unalmzl.edu.co).

Degg, M. 1993: Earthquake, hazard, vulnerability and response. *Geography* 78, 165-170.

De Silva, D. G., Kruse, J. B., and Y. Wang, 2004: Catastrophe-Induced Destruction and Reconstruction. *Natural Hazards Review* 7(1), 19-25.

De Silva, D. G., Kruse, J. B., and Y. Wang, 2008: Spatial Dependencies in wind-related housing damage. *Natural Hazards Review* 47(3), 317-330.

Donner, W., 2007: The political ecology of disaster: an analysis of factors influencing U.S. tornado fatalities and injuries, 1998-2000, *Demography* 44(3), 669-685.

Doswell, III, C. A., and D. W. Burgess, 1988: Some Issues of United States tornado climatology, *Monthly Weather Review* 116, 495-501.

Doswell, III, C. A., 2003: Societal impacts of severe thunderstorms and tornadoes: lessons learned and implications for Europe, *Atmospheric Research* 67–8, 135–152.

Doswell, III, C. A., 2005: Progress toward developing a practical societal response to severe convection (2005 EGU Sergei Soloviev Medal Lecture). *Natural Hazards and Earth System Science* 5, 691-702.

Doswell, III, C. A., Brooks, H. E., and N. Dotzek, 2009: On the implementation of the enhanced Fujita scale in the USA. *Atmospheric Research* 93(1-3), 554-563.

Dotzek, N., Grieser, J., and H. E. Brooks, 2003: Statistical modeling of tornado intensity distributions. *Atmospheric Research* 67-68, 163-187.

Dunford, M., and L. Li. 2011: Earthquake reconstruction in Wenchuan: Assessing the state overall and addressing the ‘forgottern phase’. *Applied Geography* 31(3), 998-1009.

Eckhardt, D.W., J.P. Verdin and G.R. Lyford. 1990: Automated Update of an Irrigated lands GIS Using SPOT HRV Imagery. *Photogrammetric Engineering & Remote Sensing*56(11): 1515-1522.

El-Sabh, M. I., Murty, T. S., Venkatesh, S., Siccardi, F., and K. Andah, 1990: Recent Studies in Geophysical Hazards. *Advances in Natural and Technological Hazards Research* 3, 260.

Engvall, J.L., Tubbs, J.D. and Q. A. Holmes, 1977: Pattern recognition of Landsat data based upon temporal trend analysis. *Remote Sensing Environment* 6, 303–314.

Etkin, D., Haque, E. Bellisario, L. and I. Burton, 2004: *An Assessment of Natural Hazards and Disasters in Canada: The Canadian Natural Hazards Assessment Project*. Public Safety and emergency preparedness Canada and environment Canada, Ottawa.

Finch, C., Emrich, C. T. and S. L. Cutter, 2010: Disaster disparities and differential recovery in New Orleans. *Population Environment* 31(4), 179-202.

Fontaine, M.M. and A. C. Steinemann. 2009: The determinants of vulnerability and adaptive capacity at the national level and the implications for adaptation. *Natural Hazards Rev*iew 10(1), 11-18.

Fujita, T. T., 1971: Proposed characterization of tornadoes and hurricanes by area and intensity. SMRP Research Rep. 91, University of Chicago, Chicago, IL., 15 pp.

Fujita, T. T., 1973: Experimental classification of tornadoes in FPP scale. SMRP Research Rep. 98, University of Chicago, Chicago IL., 15 pp.

Fujita, T. T. 1981: Tornadoes and downbursts in the context of generalized planetary scales. *Journal of Atmospheric Science* 38, 1511-1534.

Fujita, T. T. and B. E. Smith, 1993: Aerial survey and photography of tornado and microburst damage. *The Tornado: Its Structure, Prediction and Hazards*. *Geophys. Monogr*. No. 79, Amer. Geophys. Union, 479 - 493.

Fussel, H. M., 2007: Vulnerability: A generally applicable conceptual framework for climate change research. Global Environmental Change 17(2), 155-167.

Gilabert, M.A., Gonzales-Piqueros, J., Garcia-Haro, F.J. and J. Melia, 2002: A generalized soil-adjusted vegetation index. *Remote Sensing of Environment* 82, 303–310.

Gitas, I. Z., Polychronaki, A., Katagis, T., and Malinis, G., 2008: Contribution of remote sensing to disaster management activities: A case study of the large fires in the Peloponnese, Greece, *International Journal of Remote Sensing* 29(6), 1847–1853.

Grazulis, T. P. 1991: *Significant Tornadoes, 1880–1989, Volume 1: Discussion and Analysis*. Environmental Films.

Grossman, L., 1977: Man-environment relationships in anthropology and geography. *Annals of the Association of American Geographers* 67(1), 126-144.

Hall, F. G., D.E. Strebel, J.E. Nickeson and S.J. Goetz . 1991: Radiometric rectification: towards a common radiometric response among multidate, multisensor Images. *Remote Sensing of the Environment* 35(1), 11-27.

Hansen, M.C., Roy D. P., Lindquist, E., Adusei, B., Justice, C. O., and A. Altstatt, 2008: A method for integrating MODIS and Landsat data for systematic monitoring of forest cover and change in the Congo Basin. *Remote Sensing of Environment, Earth Observations for Terrestrial Biodiversity and Ecosystems Special Issue* 112(5), 2495-2513.

Hass, P., Eugene, K. and W. Robert, 1977: *Reconstruction Following Disaster*. Bowden MJ editors, MIT University Press, Cambridge.

Heneka, P. and B. Ruck, 2008: A damage model for the assessment of winter storm damage to buildings. *Engineering Structures* 30(12), 3603–3609.

Hewitt, K., I. Burton, 1971: *The Hazardousness of a Place: A Regional Ecology of Damaging Events*. Department of Geography Research publication 6, University of Toronto, Toronto, Canada.

Hord, R. M. and W. Brooner., 1976: Land-use map accuracy criteria. *Photogrammetric Engineering and Remote Sensing* 42, 671-677.

Huete, A. R., 1988: A soil-adjusted vegetation index (SAVI). *Remote Sensing of Environment* 25**,** 295–309.

Islam, M.M. and K. Sado, 2000: Flood hazard assessment in Bangladesh using NOAA-AVHRR images with Geographic Information System, *Hydrological Processes* 14, 605-620.

Jedlovec, G. J., Nair, U. and S. L. Haines, 2006: Detection of storm damage tracks with EOS data. *Weather and Forecasting* 21, 249 - 267.

Jensen, J. K. Rutchey, M.S. Koch and S. Narumalani, 1995: Wetland Change Detection in the Everglades Water Conservation Area 2A Using a Time Series of Normalized Remotely Sensed Data, *Photogrammetric Engineering & Remote Sensing* 61(2): 199-209.

Jensen, J.R. 1996: *Introductory to Digital Image Processing: A Remote Sensing Perspective*. Prentice-Hall. Saddle River, New Jersey.

Joyce, K. E., Belliss, S., Samsonov, S., McNeill, S., and P. J. Glassey, 2009: A review of the status of satellite remote sensing image processing techniques for mapping natural hazards and disasters. *Progress in Physical Geography* 113(8), 183-207.

Kawamura, M., S. Jayamamana and Y. Tsujiko, 1997: Comparison of Urbanization and Environmental Condition in Asian Cities using Satellite Remote Sensing Data. Available online:http://www.gisdevelopment.net/aars/acrs/1997/ps1/ps2008.shtml.

Kaplan, M., Renaud, F. G., and Lüchters, G., 2009: Vulnerability assessment and protective effects of coastal vegetation during the 2004 Tsunami in Sri Lanka. *Natural Hazards and Earth System Sciences* 9(4), 1479-1494.

Kauth, R. J. and G. S. Thomas, 1976. The Tasseled Cap -- A Graphic Description of the Spectral-Temporal Development of Agricultural Crops as Seen by LANDSAT, *LARS Symposia.* Paper 159.

Klein, Richard J. T., Nicholls, Robert J., and F. Thomalla, 2003: Resilience to natural hazards: How useful is this concept?, *Global Environmental Change Part B: Environmental Hazards* 5(1-2), 35-45.

Klemas, V., 2009: The role of remote sensing in predicting and determining coastal storm impacts. *Journal of Coastal Research* 25, 1264–1275.

Lee, M., Lin, T., Vadeboncoeur, M., and J. Hwong, 2008: Remote sensing assessment of forest damage in relation to the 1996 strong typhoon Herb at Lienhuachi Experimental Forest, Taiwan. *Forest Ecology and Management* 255, 3297–3306.

Lewis, J., 1987: Risk, Vulnerability, and survival: some post-Chernobyl implications of people, planning, and civil defense. *Local Government Studies July/August*, 75-93.

Lewis, J., 1990: The vulnerability of small island states to sea level rise: the need for holistic strategies. *Disasters* 14, 241-249.

Lillesand, T.M. and R.W.Keifer, 1979: Remote Sensing and Image Interpretation. Second Edition, John Wiley & Sons.

Lillesand, T.M., Kiefer, R.W. and J. W. Chipman. 2004: *Remote sensing and image interpretation* (fifth edition). Chichester: Wiley, 763 pp.

Lin, C.W., Shieh, C.L., Yuan, B.D., Shieh, Y.C., Liu, S.H., and S. Y. Lee, 2004: Impact of the Chi-Chi earthquake on the occurrence of landslides and debris flows: Example from the Chenyulan River watershed. *Engineering Geology* 71, 49–61.

Lin, C.Y., Lo, H.M., Chou, W.C. and W.T. Lin, 2004: Vegetation recovery assessment at the Jou-Jou Mountain landslide area caused by the 921 Earthquake in central Taiwan. *Ecology Model* 176, pp. 75–81.

Liverman, D., 1990: Drought Impacts in Mexico: Climate, Agriculture, Technology, and Land Tenure in Sonora and Puebla. *Annals of the Association of American Geographer* 80(1), 49-72.

Longhurst, R., 1995: The assessment of community vulnerability in hazard prone areas, conference report. *Disasters* 19, 269-270.

Lu, D., Batistella, M., Moran, E., and P. Mausel, 2004: Application of spectral mixture analysis to Amazonian land-use and land-cover classification, *International Journal of Remote Sensing* 25, 5345–5358.

Lunetta, R. S.,and C. D.Elvidge, 1998: Remote *sensing change detection*. MI: Ann Arbor Press.

Magsig, M., M. Dickens-Micozzi, and M. Yuan, 2000: Analysis of tornado damage on May 3rd, 1999, using remote sensing and high-resolution satellite imagery. *Preprints, 20th Conf. on Severe Local Storms, Orlando, FL, American Meteorological Society*, 9–12.

Mahiny, A.S. and B. Turner, 2007: A comparison of four common atmospheric correction methods. *Photogrammetric Engineering & Remote Sensing* 73(4), 361–368.

Marshall, T. P., 2002: Tornado damage survey at Moore, Oklahoma. *Weather and Forecasting* 30(4), 433-450.

Manyena, S. B., 2006: The concept of resiliency revisited. *Disasters* 17, 582–598.

McCarthy, D. W., 2003: NWS tornado surveys and the impact on the national tornado database. Preprints, *First Symp. on F-Scale and Severe-Weather Damage Assessment,* Long Beach, CA, American Meteorological Society, CD-ROM, 3.2.

McDonald, J. R., 2002: Development of an enhanced Fujita scale for estimating tornado intensity. *Preprints 21st Conf. on Severe Local Storms, Austin*. *American Meteorological Society*, Boston, 174–177.

Mileti, D., 1999: *Disasters by Design: A Reassessment of Natural Hazards in the United States*. Washington, D.C.: Joseph Henry Press.

Mitchell, J.K., 1989: *Hazards research*. In Gaile, G.L. and Willmott, C.J., editors, Geography in America, Columbus, OH: Merrill, 410-424.

Mitchell, J.K. 1999: *Crucibles of Hazard: Mega-Cities and Disasters*. Tokyo, United Nations University Press.

Mura, D. M., Benediktsson, J. A., Bovolo, F. and L. Bruzzone, 2008: An unsupervised technique based on morphological filters for change detection in very high resolution images, *Geoscience Remote Sensing Letters* 5(3), 433–437.

Myers, C., Slack, T., and J. Singleman, 2008: Social vulnerability and migration in the wake of disaster: the case of Hurricanes Katrina and Rita. *Population Environment* 29, 271-291.

Myint, S. W and L. Wang, 2006: Multi-criteria Decision Approach for Land Use Land Cover Change Using Markov Chain Analysis and Cellular Automata Approach, *Canadian Journal of Remote Sensing* 32(6), 390-404.

Myint, S., Yuan, M., Cerveny, R. and C. Giri. 2008: Categorizing Natural Disaster Damage Assessment using Satellite-based Geospatial Techniques. *Natural Hazards and Earth Systems Sciences* 8, 707–719.

Myint, S., Yuan, M. Cerveny, R. and C. Giri, 2008: Comparison of Remote Sensing Image Processing Techniques to Identify Tornado Damage Areas from Landsat TM Data. *Sensors* 8, 1128–1156.

Myint, S.W., Giri, C. P., Wang, L., Zhu, Z., & Gillette, S. (2008). Identifying mangrove species and their surrounding land use and landcover classes using an object oriented approach with a lacunarity spatial measure. *GIScience and Remote Sensing* 45, 188−208.

National Climate Data Center. 2010: http://www4.ncdc.noaa.gov/cgi win/wwcgi.dll?wwEvent~Storms

National Climate Data Center.2010b: http://www.ncdc.noaa.gov/oa/climate/severeweather/tornadoes.html

Oklahoma Climatological Survey. 2010.

http://climate.mesonet.org/county_climate/Products/oklahoma_climate_overview.pdf

Oklahoma Climatological Survey. 2010b. http://climate.mesonet.org/climate_trends.html

Pan, K., Montpelier, P., and M. Zadeh, 2002: Engineering observations of 3 May 1999 Oklahoma tornado damage. *Weather and Forecasting* 17, 599-610.

Paul, B., 2005: Evidence against disaster-induced migration: the 2004 tornado in north-central Bangladesh. *Disasters* 29(4), 370-385.

Peterson, C.J., 2000: Damage and recovery of tree species after two different tornadoes in the same old growth forest: A comparison of infrequent wind disturbances. *Forest Ecology Management* 135(1–3), 237–252.

Preston, V., Tylor, S. M., and D. C. Hodge, 1983: Adjustments to natural and technological hazards: a study of urban residential community. *Environmental Hazards* 15(2), 143-164.

Quarantelli, E. L., 1998: *What is a disaster? Perspectives on the question.* London/ New York: Routledge.

Rejaie, A. and M. Shinozuka, 2004: Reconnaissance of Golcuk 1999 earthquake damage using satellite images, *Journal of Aerospace Engineering* 17(1), 20–25.

Roemer, H., Jeewarongkakull, J., Kaiser, G., Ludwig, R., and H. Sterr, 2011: Monitoring post-tsunami vegetation recovery in Phang-Nga province, Thailand – a remote sensing based approach. *International Journal of Remote Sensing* Preprint.

Rouse, J.W., Haas, R.H., Schell, J.A. and Deering, D.W., 1973. Monitoring vegetation systems in the Great Plains with ERTS. In: Freden, S.C., Mercanti, E.P. and Becker, M., Editors, 1973. *Third Earth Resources Technology Satellite-1 SymposiumTechnical presentations, section A* 1, National Aeronautics and Space Administration, Washington, DC, pp. 309–317 NASA SP-351.

Sabins, F.F., 1997. Remote Sensing — Principles and Interpretation, 3rd edition, W.H. Freeman, New York, NY., 494 pp.

Schaefer, J. T., Schneider, R. S. and M. P. Kay, 2002: The robustness of tornado hazard estimates. Preprints, *Third Symp. on Environmental Applications,* Orlando, FL, *American Meteorological. Society*, 35–41.

Singh, A. and A. Harrison, 1985: Standardized principal components.

International Journal of Remote Sensing 6, 883-896.

Singh, A, 1989: Digital change detection techniques using remotely sensed data. *International Journal of Remote Sensing* 10, 998-1003.

Simmons, K., 2007: Tornado Shelters and manufactured home parks market. *Natural Hazards* 43, 365-378.

Speheger, D. A., Doswell, III, C. A., and G. J. Stumpf, 2002: The tornadoes of 3 May 1999: event verification in Central Oklahoma and related issues. *Weather and Forecasting* 17(3), 362-381.

Sun, W. and S. Okubo, 2004: Coseismic deformations detectable by satellite gravity missions: a case study of Alaska (1964, 2002) and Hokkaido (2003) earthquakes in the spectral domain, *Journal of Geophysical Research, [Solid Earth]* 109.

Tierney, K. and M. Bruneau, 2007: Conceptualizing and measuring resilience: a key to disaster loss reduction, *TR News May–June*, pp. 14–17.

Timmerman, P., 1981: *Vulnerability, Resilience and the Collapse of Society: A Review of Models and Possible Climatic Applications*. Institute for Environmental Studies, University of Toronto, Canada.

Townshend, J.R.G., Justice, C.O., Gurney, C., McManus, J., 1992: The impact of misregistration on change detection, *Geoscience and Remote Sensing*, 30(5), 1054 – 1060.

Turner, B.A., 1976: The Organizational and Interorganizational Development of Disaster. *Administrative Science Quarterly* 21(3), 378-397.

Turner, B. L., Kasperson, R., Matson, P. A., McCarthy, J. J., Corell, R. W., Christensen, L., Eckley, N., Kasperson, J. X., Luers, A., Martello, M. L., Polsky, C., Pulsipher, A., and A. Schiller, 2003: A Framework for Vulnerability Analysis and Sustainability Science, *Proceedings of the National Academy of Sciences 100*, 8074–8079.

Uitto, J., 1998: The geography of disaster vulnerability. *Applied Geography* 18(1), 7-16.

Villa, P., 2007: Imperviousness indexes performance evaluation for mapping urban areas using remote sensing data. *Joint Urban Remote Sensing Event*, Paris 11-13 , 1-6.

Wang, W., Qu, J. J., Hao, X., Liu, Y. and J. A. Stanturf, 2010: Post-hurricane

forest damage assessment using satellite remote sensing. *Agricultural and Forest Meteorology* 150, 122-132.

Wang, Y., Colby, J. D., and K. A. Mulcahy, 2002: An efficient method for mapping flood extent in a coastal floodplain using Landsat TM and DEM data, *International Journal of Remote Sensing* 23(18), 3681–3696.

Wentz, E.A., Stefanov, W.L., Netzband, M., Moller, M., and A. J. Brazel. 2009: Global Mapping of Human Settlements: Experiences, Datasets, and Prospects. 191-204.

Wilhite, D., and W. Easterling, 1987: *Planning for Drought: Toward a Reduction of Societal Vulnerability*. Boulder, Colorado, Westview Press.

Wilkinson, D. W., and M. K. Crosby, 2010: Rapid Assessment of Forest Damage from Tornadoes in Mississippi. Boulder, *Photogrammetric Engineering and Remote Sensing* 76(12), 1298-1301.

Yasui, E., 2007: Community Vulnerability and capacity in post-disaster recovery: the cases of Mano and Mikura neighborhoods in the wake of the 1995 Kobe Earthquake. Unpublished Ph.D. dissertation for the University of British Colombia.

Yuan, M., Dickens-Micozzi, M., and M. A. Magsig, 2002: Analysis of tornado damage tracks from the 3 May tornado outbreak using multispectral satellite imagery. *Weather and Forecasting* 17(3), 382-398.

Zhou, H., Wang, J., Wan, J. and H. Jia, 2010, Resilience to natural hazards: a geographic perspective. *Natural Hazards* 53(1), 21-41.